https://doi.org/10.5194/egusphere-2026-6051
Preprint. Discussion started: 18 November 2026
© Author(s) 2026. CC BY 4.0 License.

Linking high-frequency (T ≤ 3 h) sea level and atmospheric pressure extremes in the middle Adriatic: a multi-year observational study

Nikola Metličić[1], Jadranka Šepić[1], Hrvoje Mihanović[2]

[1]Faculty of Science, University of Split, 21000 Split, Croatia
[2]Institute of Oceanography and Fisheries, 21000 Split, Croatia

Correspondence to: Nikola Metličić (nmetlicic@pmfst.hr)

Abstract. High-frequency (HF) sea level oscillations (T ≤ 3 h), including meteotsunamis, represent a significant coastal hazard along the eastern Adriatic coast. Funnel-shaped bays and harbours in the region are particularly susceptible to amplification of incoming long ocean waves through harbour resonance and shoaling, following their offshore generation and amplification via Proudman and/or Greenspan resonance. Despite growing awareness of this hazard, the statistical relationship between atmospheric pressure disturbances and extreme sea level responses across the region remains insufficiently quantified. In this study, the spatiotemporal relationship between HF atmospheric pressure and HF sea level extremes was investigated using an observational network of five tide-gauge and nine microbarograph stations strategically distributed across the eastern and western coasts of the middle Adriatic. The measurements span May 2017 to October 2024, providing up to 7.4 years of simultaneous 1-minute sea level and air pressure observations. Extreme sea level and atmospheric pressure episodes were identified using wave-height and normalised moving variance (NMV) thresholds, respectively, and their relationships were analysed across the regional network. Between 80 and 100% of extreme sea level episodes were associated with an HF atmospheric pressure extreme at one or more microbarograph stations, with connection rates generally increasing for stronger sea level episodes. Conversely, only 32–45% of extreme atmospheric pressure episodes were associated with an extreme sea level response. Stronger atmospheric disturbances were generally associated with larger sea level wave heights, although substantial overlap between intensity classes showed that atmospheric pressure intensity alone was insufficient to explain the observed wave heights. Time-lag analysis indicated that atmospheric disturbances predominantly approached from westerly directions, with their propagation velocities inferred from median time lags between the peak sea level oscillation of each sea level episode at each tide gauge and the nearest extreme HF air pressure NMV point at the available microbarograph stations, ranging from ~12 to 20 m s^{-1}, depending on the tide-gauge station. Simultaneity analyses showed that extreme sea level episodes occurred concurrently across the middle Adriatic, with simultaneity exceeding 50% for most station pairs, while the strongest atmospheric disturbances tended to affect a larger portion of the region concurrently (simultaneity exceeding 50% for most station pairs) than weaker atmospheric extremes (simultaneity exceeding 30% for most station pairs). These results provide an additional observational basis for meteotsunami forecasting and early warning systems in the middle Adriatic region.

https://doi.org/10.5194/egusphere-2026-6051
Preprint. Discussion started: 18 November 2026
© Author(s) 2026. CC BY 4.0 License.

1 Introduction

High-frequency (HF) sea level oscillations, occurring on periods from a few minutes to several hours, have received increasing attention in the oceanographic community in recent years. This growing interest largely reflects the increasing availability of 1-minute sea level time series (Zemunik et al., 2021). HF sea level oscillations encompass a broad range of phenomena, including seismic tsunamis (Pugh and Woodworth, 2014), meteotsunamis (Monserrat et al., 2006), seiches (Rabinovich, 2009), edge waves (Munk et al., 1956), infragravity waves (Munk, 1949; Aucan and Ardhuin, 2013; Medvedev et al., 2022), and wind waves (Dodet et al., 2019). All of these can significantly contribute to extreme sea levels and coastal hazards (Pugh and Woodworth, 2014).

Further on, their impacts are expected to become increasingly important due to ongoing sea level rise and its projected acceleration under climate change scenarios (Woodworth et al., 2011; Nerem et al., 2018). Additionally, rather than acting in isolation, these phenomena can coincide with each other and with longer period extremes such as storm surges, further increasing severity of coastal flooding (Medvedev et al., 2022).

Among HF sea level oscillations, meteorological tsunamis (meteotsunamis) represent one of the most notable and hazardous phenomena (Rabinovich and Monserrat, 1998; Jansà et al., 2007; Orlić et al., 2010; Linares et al., 2019). Their underlying physics is well understood and documented (Vilibić et al., 2025). These long ocean waves typically occupy periods from a few minutes to several hours and are generated by rapid and intense atmospheric pressure disturbances (Monserrat et al., 2006; Vilibić and Beg Paklar, 2006; Vilibić and Šepić, 2009). Such disturbances are commonly associated with atmospheric gravity waves (Belušić et al., 2007; Jansà and Ramis, 2021; Šepić et al., 2009, 2015b), thunderstorms (Belušić and Strelec Mahović, 2009; Wijeratne and Pattiaratchi, 2024), squall lines, frontal passages, and cyclonic activity (Bechle et al., 2015; Haslett et al., 2009; Šepić and Rabinovich, 2014; Heidarzadeh and Rabinovich, 2021; Medvedev et al., 2022).

The atmospheric forcing responsible for meteotsunami generation can persist from tens of minutes to several hours (Vilibić et al., 2025) and even days (Šepić and Rabinovich, 2014), while the resulting long ocean waves may be amplified through several resonant mechanisms. These include Proudman resonance (Proudman, 1929; Orlić, 1980) which occurs when the speed of a travelling atmospheric disturbance matches the speed of long ocean waves over a shelf of near-uniform depth (Vilibić et al., 2004; Vilibić, 2008); Greenspan resonance (Greenspan, 1956) which occurs when the along-coast propagation speed of the atmospheric disturbance matches that of ocean edge waves (Niu, 2020, 2021; Seo and Liu, 2014); and harbour resonance (Raichlen, 1966; Rabinovich, 2009) which occurs when the frequency of incoming long ocean waves coincides with the natural frequency of a harbour or a bay. Additional amplification occurs as long ocean waves enter shallow and narrowing harbours and bays, where shoaling further increases their height (Lamb, 1932; Monserrat et al., 2006; Pattiaratchi and Wijeratne, 2015). The required combination of atmospheric forcing characteristics, bathymetry, coastline geometry, and resonant conditions explains why destructive meteotsunamis are rare and restricted to specific locations (Jansà and Ramis, 2021; Vilibić et al., 2025).

https://doi.org/10.5194/egusphere-2026-6051
Preprint. Discussion started: 18 November 2026
© Author(s) 2026. CC BY 4.0 License.

Meteotsunamis have been documented worldwide, with many regions developing their own terminology and definitions for these events (summarised in Vilibić et al., 2025). Well-known examples include the Balearic Islands in the Mediterranean, Malta, Sicily, the United Kingdom, the Black Sea, the Baltic Sea, the Great Lakes, the eastern coasts of the USA and Canada, Nagasaki Bay in Japan, the Yellow Sea, the East China Sea, and Australia (Vilibić et al., 2025 and references therein). Among these regions, the Adriatic Sea is recognised as one of the major meteotsunami hotspots (Vilibić et al., 2016; Rabinovich, 2020). Considerable effort has gone into cataloguing historical events in the region (Orlić, 2015; Šepić and Orlić, 2026), documenting some of the most severe cases on record. These include a few middle Adriatic events such as the Vela Luka event of 21 June 1978 (Orlić, 1980; Vučetić et al., 2009; Orlić et al., 2010), during which wave heights of 6 meters were witnessed at the head of the bay, and the 27 June 2003 meteotsunami event, which affected both Stari Grad on Hvar Island and Mali Ston Bay (Vilibić et al., 2004; Monserrat et al., 2006). These events resulted in significant structural damage, coastal flooding, and destruction of local shellfish farms.

Although numerous case studies have documented meteotsunami generation and resonance in the Adriatic and have attempted to reconstruct individual events, including estimates of the propagation speed and direction of the associated atmospheric disturbances (Vilibić et al., 2004; Vilibić and Šepić, 2009; Orlić et al., 2010; Šepić et al., 2009, 2012, 2015a, 2016; Denamiel et al., 2018; Bubalo et al., 2018; Tojčić et al., 2021), far less attention has been paid to systematically linking HF sea level episodes with the HF atmospheric disturbances and their spatial distribution, timing, and intensity characteristics. Villalonga et al. (2024) investigated the atmospheric disturbances associated with meteotsunamis in Ciutadella, characterising their propagation speed and direction, spectral content, and spatial structure. They found that the largest sea level oscillations occurred when the propagation characteristics of the atmospheric disturbances were more homogeneous in space and time, although no empirical relationship between atmospheric features and sea level oscillation amplitudes could be established. Subsequently, Villalonga et al. (2026) extended the analysis to a regional scale across the Balearic Islands, using observations from 27 tide gauges to characterise the spatial distribution and occurrence of meteotsunamis. These two papers highlighted the importance of both regional atmospheric forcing and local resonant amplification. However, a comparable systematic assessment of the relationship between HF sea level and atmospheric pressure oscillations has not yet been conducted in the middle Adriatic.

Ruić et al. (2023) analysed 1-minute sea level time series from 18 tide-gauge stations (with series length ranging from 2.9 to 17.5 years) distributed evenly along the eastern and western Adriatic coasts and showed that HF sea level oscillations significantly contribute to recorded Adriatic Sea extremes, particularly over the middle Adriatic. This is also the region where most of the known Adriatic Sea meteotsunamis have been observed (29 out of 36 events listed in the on-line version of Adriatic Sea meteotsunami catalogue; Šepić and Orlić, 2026). The middle Adriatic extends southward from the shallow northern Adriatic shelf, across the Jabuka Pit, to just north of the deep South Adriatic Pit (Fig. 1). The region is characterised by pronounced bathymetry changes (depths up to 270 m), numerous islands, channels, and funnel-shaped bays with high amplification factors, providing favourable conditions for long wave amplification through Proudman resonance over suitable depth ranges, as well as harbour resonance (Vilibić et al., 2004; Vilibić and Šepić, 2009; Denamiel et al., 2018).

https://doi.org/10.5194/egusphere-2026-6051
Preprint. Discussion started: 18 November 2026
© Author(s) 2026. CC BY 4.0 License.

As already noted, the connection between atmospheric disturbance and meteotsunamis has been established in previous research for selected meteotsunami events. The middle Adriatic meteotsunamis were commonly generated by atmospheric pressure disturbances characterised by a rate of air pressure change mostly higher than 1 hPa over 5 minutes, propagating from southwest-west-northwest directions with likely speed range from 15 to 50 m s^{-1} (Šepić and Vilibić, 2011; Šepić et al., 2016; Šepić and Orlić, 2026) and causing strongest meteotsunamis at westward-facing harbours located along the eastern Adriatic coast (Pupić Vurilj et al., 2023; Vilibić et al., 2021; Šepić and Orlić, 2026). These atmospheric disturbances typically propagated with speed and direction of the mid- and upper-troposphere winds (e.g., Šepić et al., 2015b). Vilibić and Beg Paklar (2006) and Vilibić (2008) demonstrated, through a series of numerical experiments, the importance of the speed and direction of travelling atmospheric disturbances, both of which directly control the energy transfer to the sea via resonant coupling.

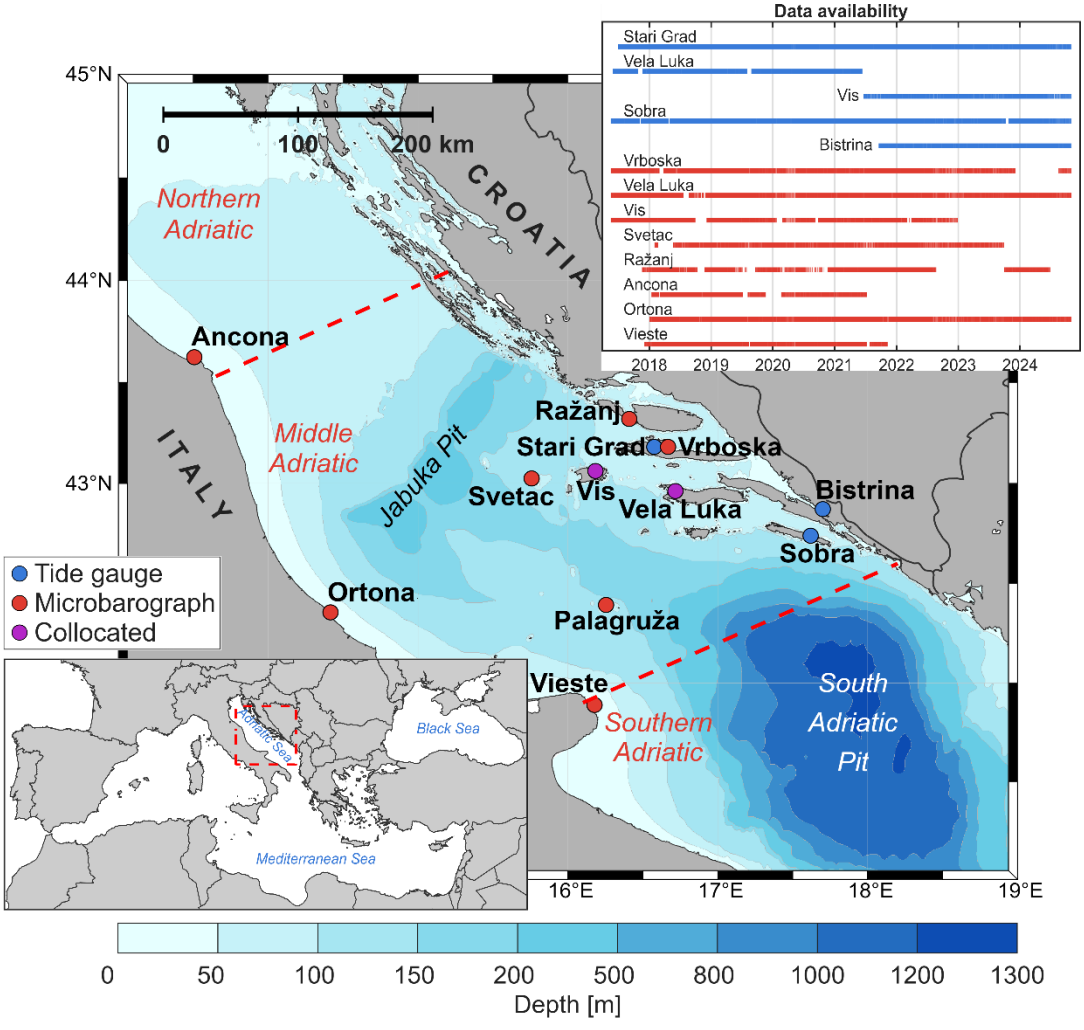


Figure 1. Study area and the bathymetry of the Adriatic Sea with locations of tide-gauge (blue circles) and microbarograph stations (red circles). The Adriatic is divided into three parts with red dashed lines: northern, middle and southern. The position of the Adriatic Sea relative to the Mediterranean is shown in the bottom left inset. The top right inset shows the availability of sea level and air pressure time series.

https://doi.org/10.5194/egusphere-2026-6051
Preprint. Discussion started: 18 November 2026
© Author(s) 2026. CC BY 4.0 License.

Herein, we expand the existing knowledge by systematically investigating the relationship between extreme HF sea level oscillations and HF atmospheric pressure disturbances in the middle Adriatic. To do so, we use long-term (3 to 7.5 years) simultaneous observations from five tide-gauge and nine microbarograph stations (locations shown in Fig. 1). The study includes tide gauges at Stari Grad, Vela Luka, and Mali Ston Bay, i.e., at locations where HF sea level oscillations have been extensively studied and where strong meteorological tsunamis have previously been observed, as well as tide gauges at Vis and Sobra. Although the strongest HF sea level oscillations in the study region are generally associated with meteotsunami events, the present analysis does not explicitly distinguish meteotsunamis from other HF oscillations. We therefore define and analyse HF sea level episodes exceeding a prescribed wave-height-based threshold, acknowledging that some of these episodes would elsewhere be classified as meteotsunamis, while here we refer to them collectively as extreme HF sea level episodes. The study thus characterises the occurrence and intensity of extreme HF sea level and HF atmospheric pressure episodes, quantifies their temporal and spatial correspondence across the observational network and provides an initial estimation of the propagation characteristics of atmospheric disturbances associated with the extreme HF sea level episodes.

The remainder of the paper is organised as follows. In Sect. 2 we describe the study area, the datasets and the methodology, including spectral analysis. Section 3 presents the results across six subsections. In Sect. 3.1 we give an overview of the general statistics of the HF extremes identified in both sea level and atmospheric records. In Sect. 3.2 we examine the connections between extreme HF sea level episodes and extreme HF air pressure episodes, taking sea level series as the reference ones. In Sect. 3.3 we analyse how HF air pressure intensity varies across different wave-height intensity classes. Section 3.4 assesses general propagation characteristics of atmospheric disturbances associated with the observed HF sea level episodes. In Sect. 3.5 we invert the analysis of Sect. 3.2, examining the connections between extreme HF air pressure episodes and extreme HF sea level episodes with air pressure series taken as the reference one. Section 3.6 characterises HF sea level intensity across classes of HF air pressure intensity. We discuss research findings in Sect. 4 and Sect. 5 presents the main concluding remarks.

2 Materials and methods

This study is based on simultaneous sea level and air pressure measurements collected from a network of tide-gauge (TG) and microbarograph (MB) stations in the middle Adriatic Sea. The studied stations include five TG stations, Stari Grad (Hvar Island), Vela Luka (Korčula Island), Vis (Vis Island), Sobra (Mljet Island), and Bistrina (Mali Ston Bay), all five in Croatia, and nine MB stations, including six stations located in Croatia, in Vrboska (Hvar Island), Vela Luka (Korčula Island), Vis (Vis Island), Svetac (Svetac Island), Ražanj (Brač Island), Palagruža (Palagruža Island), and three stations located on the Italian mainland, Ancona, Ortona, and Vieste. Most of these stations were installed precisely for tracking meteotsunami generation and propagation and for the establishment of a meteotsunami early warning system within the Institute of Oceanography and Fisheries projects dedicated to meteotsunami research. Figure 1 shows the bathymetry of the Adriatic Sea together with the locations of the TG and MB stations used in this study. The stations are predominantly distributed across the middle Adriatic region, which is recognised as a hotspot for meteotsunami activity (Vilibić and Šepić, 2009; Šepić et al., 2016; Šepić and Orlić,

https://doi.org/10.5194/egusphere-2026-6051
Preprint. Discussion started: 18 November 2026
© Author(s) 2026. CC BY 4.0 License.

2026). The configuration of the network enables direct comparison between collocated and more distant station pairs and allows us to investigate how the relationship between atmospheric forcing and sea level response holds up across different distances and directions.

Sea level was measured using radar-type TG stations with a 1-minute sampling step and 0.1 cm resolution, while air pressure was recorded by high-precision MB stations (0.01 hPa resolution) with a 1-second sampling step. The air pressure data are stored locally at station and then transmitted hourly to a central unit, where 1-minute averages are computed and stored. We used these 1-minute averages in our analyses. Data can be visualised at http://faust.izor.hr/autodatapub/postaje. The analysed sea level and air pressure measurements span the period from 17 May 2017 to 31 October 2024, with the Sobra TG series defining the start of simultaneous sea level and air pressure observations. The lengths of the available time series vary between stations (Fig. 1, inset), ranging from approximately 3.1 to 7.4 years (Table 1).

2.1 Data quality control

We applied comprehensive quality control to the sea level and air pressure series to ensure data reliability. For sea level data, we first removed extreme out-of-range values using station-specific thresholds determined by visual inspection, varying from 76 to 105 cm. We then applied an automated procedure to detect outliers based on differences between neighbouring measurements, removing values that differed by more than 50 cm from one neighbouring value or 30 cm from both, following methodology applied by Zemunik et al. (2021) and Balić and Šepić (2025). Additionally, we cleaned the Vela Luka and Vis sea level data using a spike detection algorithm (Williams et al., 2019), which removes values exceeding three standard deviations from a least-squares spline fit. This procedure was applied twice, as recommended. Sea level data from remaining three TGs were of higher quality, so we assessed that there was no need to clean it using this procedure. For air pressure data, we removed duplicate values which occasionally appeared in the series. Finally, we visually inspected and manually cleaned both sea level and air pressure datasets to remove any remaining outliers. Table 1 summarises the availability and quality of the datasets, showing for each station the start and end dates of measurements during the analysed period, as well as the percentage of eliminated and missing data. The percentage of eliminated data is calculated relative to the non-missing data within the time interval. Overall, the datasets are of high quality, with removed data ranging up to 0.2%, except for Vis TG (2.2%). Missing data are limited for TG stations (up to 3.4% at Vela Luka) but larger for MB stations, ranging from 2.1% (at Ortona and Vieste) to 26.1% (at Ražanj). For the Palagruža MB station, data availability is limited and overall quality is relatively poor. Consequently, we used this station only for selected cases during periods of observed extreme HF sea level episodes, for which Palagruža data were specifically processed and cleaned. During quality control, we identified certain station-specific issues. At the Svetac MB station, occasional atmospheric pressure jumps (ranging up to 8.5 hPa over 2 minutes) likely resulted from air accumulation within the instrument enclosure during strong bora or sirocco winds (not shown). At the Vis MB station, we detected a temporal drift in the recorded data, suggesting that the instrument's internal clock runs faster than real time. The estimated time offset was approximately 10 minutes in June 2021 and increased to about 18 minutes by December 2023. This estimate was obtained by comparison with data from an additional meteorological station installed at

https://doi.org/10.5194/egusphere-2026-6051
Preprint. Discussion started: 18 November 2026
© Author(s) 2026. CC BY 4.0 License.

the TG site; however, the data from this additional station were not used in the present analysis due to their lower resolution (0.1 hPa) and the relatively short record length (June 2021–October 2024). Although this drift may affect real-time applications such as early warning systems, it only slightly impacts the statistical analyses conducted in this study. Therefore, we retained the data without temporal correction. Resolving this issue properly would require on-site instrument maintenance and additional analyses.

Table 1. Availability and quality of sea level and air pressure data: start and end dates of measurements within the study period, percentage of eliminated and missing data, and length of series after eliminated and missing data are excluded; for both TG and MB stations.

	Station	Start date	End date	Eliminated data [%]	Missing data [%]	Length of series [years]
Tide gauge	Stari Grad	28.6.2017	31.10.2024	0.1	0.4	7.3
	Vela Luka	30.5.2017	12.6.2021	0.1	3.4	3.9
	Vis	20.6.2021	31.10.2024	2.2	1.2	3.3
	Sobra	17.5.2017	31.10.2024	≈0	1.5	7.4
	Bistrina	17.9.2021	31.10.2024	≈0	0.5	3.1
Microbarograph	Vrboska	17.5.2017	31.10.2024	0.1	11.9	6.6
	Vela Luka	17.5.2017	31.10.2024	≈0	3.1	7.2
	Vis	17.5.2017	28.12.2022	≈0	8.4	5.1
	Svetac	30.1.2018	29.9.2023	0.2	7.9	5.2
	Ražanj	16.11.2017	27.6.2024	0.2	26.1	4.9
	Ancona	10.1.2018	8.7.2021	0	10.4	3.1
	Ortona	1.1.2018	31.10.2024	0	2.1	6.7
	Vieste	1.12.2017	9.11.2021	≈0	2.1	3.9

2.2 Spectral analysis and signal filtering

Spectral estimates were computed using standard methods in physical oceanography (Thomson and Emery, 2024). For sea level, we calculated the spectra from de-tided series by dividing the records into overlapping 48-hour segments (2880 points) with 50% overlap. For air pressure, we applied the same procedure. The air pressure spectrum shown in Fig. 2 was obtained from the Vela Luka MB station and selected as representative, since spectral characteristics are nearly identical across all stations (not shown), consistent with general properties of atmospheric pressure variability and spatial coherence of atmospheric pressure variability over the middle Adriatic.

https://doi.org/10.5194/egusphere-2026-6051
Preprint. Discussion started: 18 November 2026
© Author(s) 2026. CC BY 4.0 License.

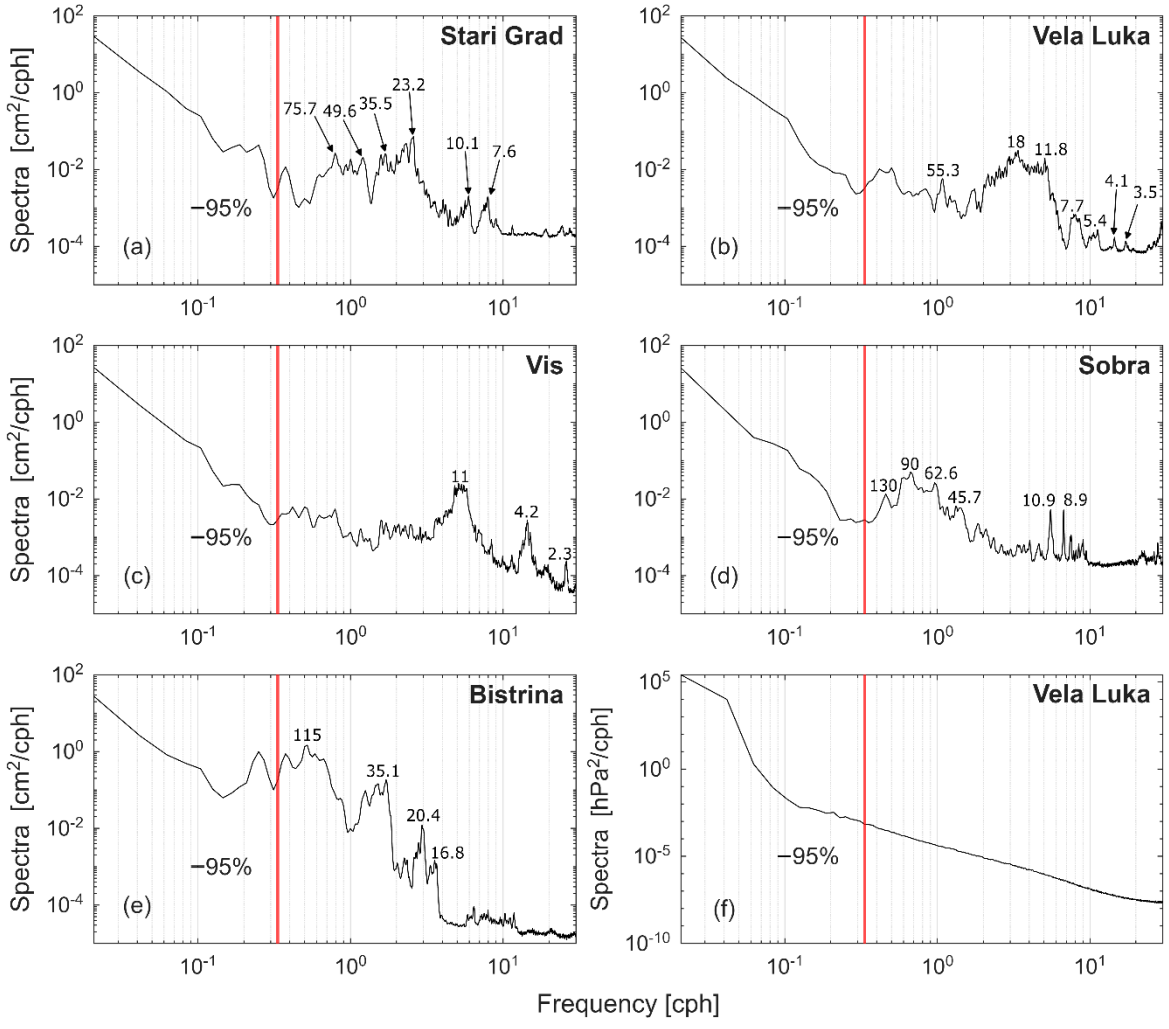


Figure 2. Spectra of sea level and air pressure time series estimated using a 48-hour window. **(a–e)** Spectra of sea level time series from all TG stations. **(f)** Spectra of air pressure time series from one representative station (Vela Luka MB). The red line marks the cut-off period of 3 hours. Sea level spectra are estimated from the residual time series. Dominant periods of sea level variability are indicated for each TG station.

To analyse HF sea level oscillations, we first removed the tidal signal using the MATLAB package T-TIDE (Pawlowicz et al., 2002), with which we estimated seven tidal harmonics, three diurnal (K1, O1, P1), and four semidiurnal (M2, S2, K2, N2). These harmonics are recognised as the ones explaining most of the Adriatic Sea tidal signal (Janeković and Kuzmić, 2005; Cushman-Roisin and Naimie, 2002; Poulain, 2013; Medvedev et al., 2020). After de-tiding, we linearly interpolated all gaps of 10 minutes or less. We then filtered the residual (de-tided) signal using a Kaiser-Bessel window of 3 hours to separate the HF and low-frequency (LF) component of sea level series (e.g., Thomson and Emery, 2024; Fig. 3). No significant spectral peaks occur at 3 hours in either sea level or air pressure spectra, i.e., this cut-off does not coincide with characteristic seiche periods at TG stations, ensuring that no relevant physical processes were artificially split or distorted (Fig. 2). The HF signal,

https://doi.org/10.5194/egusphere-2026-6051
Preprint. Discussion started: 18 November 2026
© Author(s) 2026. CC BY 4.0 License.

thus, contains sea level oscillations on time scales between 2 minutes and 3 hours and includes atmospherically induced oscillations such as infragravity waves, long ocean waves, seiches, and meteotsunamis (e.g., Vilibić and Šepić, 2017), and potentially tsunamis (e.g., Pugh and Woodworth, 2014). No seismic tsunamis occurred in the Adriatic Sea during the analysed period. Infragravity waves represent another important class of HF oscillations, typically occupying periods of 25–250 seconds (Bertin et al., 2018). They are generated primarily through nonlinear interactions of wind waves and swell (Medvedev et al., 2022) and can also contribute to extreme coastal sea levels, particularly during storm conditions (Hattori et al., 2020). Given that they occur in the Adriatic Sea (Melito et al., 2018) and that their periods partly overlap with those of meteotsunamis, caution should be exercised in distinguishing them from meteotsunamis. We applied the same 10-minute interpolation and filtering procedure to the air pressure series (Fig. 3).

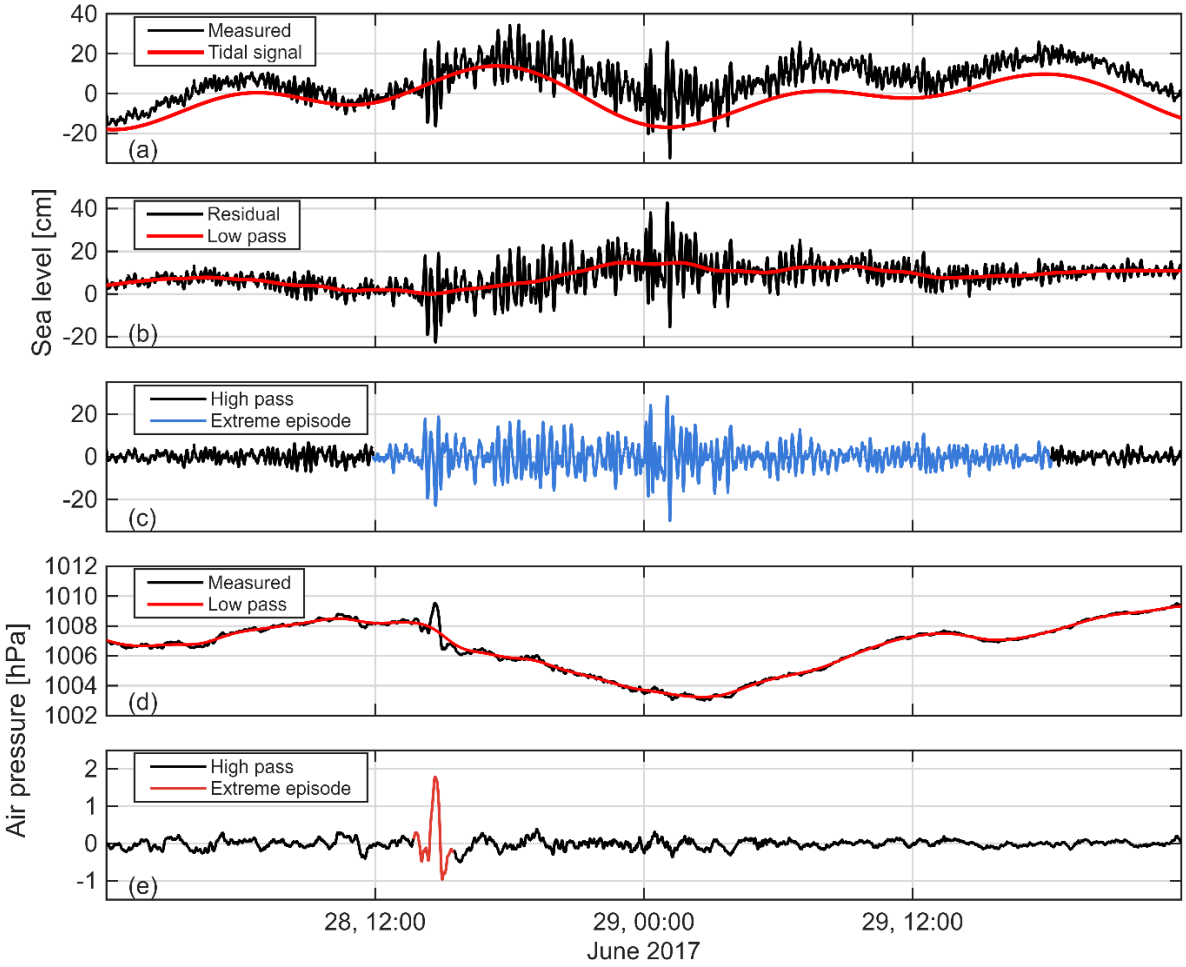


Figure 3. Example of sea level and air pressure time series. At Vela Luka TG: **(a)** measured sea level and estimated tidal signal, **(b)** residual and low-pass filtered signal, **(c)** high-pass filtered sea level signal with the extreme episode indicated. At Vrboska MB: **(d)** measured air pressure and low-pass filtered signal, **(e)** high-pass filtered air pressure signal with the extreme episode indicated. Time is given in UTC.

https://doi.org/10.5194/egusphere-2026-6051
Preprint. Discussion started: 18 November 2026
© Author(s) 2026. CC BY 4.0 License.

2.3 Identification and classification of HF sea level and air pressure extremes

We defined HF sea level extreme episodes as periods of time during which wave heights (trough-to-crest) of HF sea level series surpassed a given percentile threshold. We defined the wave heights using the zero-crossing method. To avoid splitting waves around the zero level, we applied a condition whereby a trough (crest) was disregarded if it consisted of only one point below (above) zero and if that point was less than 3 cm from zero. In this way, the larger wave height was not split in half due to small fluctuations around the zero level, keeping it as a single wave event. In addition, we removed unmatched local extrema, ensuring that two consecutive crests or troughs could not occur; in such cases, the smaller of the two adjacent extrema was discarded. This procedure ensured that each trough was paired with a corresponding crest (and vice versa).

Our sea level spectra are generally polychromatic, meaning that they contain at least two spectral peaks of comparable magnitude (Medvedev et al., 2022; Fig. 2a–e), rather than a single dominant peak. Although the zero-crossing method is more naturally suited to monochromatic (single-peaked) spectra, in our case it performed well, as it allowed us to capture the largest oscillations on which smaller-scale oscillations are superimposed, without breaking them into multiple waves. The midpoint between the trough and the crest defined the timing of the wave heights. We identified extreme HF sea level episodes using the 99.9th percentile of the wave-height distribution from each TG station. To determine the duration of an episode, we extended the episode backward and forward from each wave height exceeding the 99.9th percentile using an iterative windowing procedure. Specifically, we examined all wave heights within successive windows of 1 hour (2 hours at Sobra and Bistrina TGs because of the longer dominant oscillation periods; Fig. 2). Within each window, we identified the temporally farthest wave height exceeding the 95th percentile. If such a wave height existed, we initiated a new search window from its occurrence time and repeated the procedure. Consequently, the windows were not fixed in time but instead advanced according to the timing of the farthest wave height above the 95th percentile identified in the previous step. We continued the search until no wave height above the 95th percentile was found within the current window.

As opposed to HF sea level oscillations, which are typically wave-like (Fig. 3), HF air pressure disturbances come in various shapes, including sudden jumps, drops, individual box- or sine-like disturbances, or several wave-like oscillations. Consequently, a method based on a wave-height threshold could not be efficiently used to extract air pressure extremes. Therefore, to extract HF air pressure extremes, we first calculated a series of 15-minute moving variances and normalised them by subtracting the mean and dividing by the standard deviation of moving variances computed from all MB stations except Palagruža. To define an extreme threshold, we pooled the normalised moving variance (NMV) values from all stations (excluding Palagruža), assuming spatially coherent atmospheric forcing over the middle Adriatic (~270 × 200 km) and similar air pressure variability among stations. We defined an extreme as a 15-minute NMV exceeding the 99.9th percentile of the pooled distribution (≈ 9.5 hPa^2). To determine episode duration, we extended each extreme backward and forward in time for as long as the 60-minute NMV remained above the 98th percentile (≈ 1.4 hPa^2). We found that a 15-minute window is appropriate to capture the rapid air pressure changes capable of triggering HF sea level extremes, while the 60-minute window is better suited to determine the duration of the atmospheric disturbance, thus we used both in our analyses. We merged extreme

https://doi.org/10.5194/egusphere-2026-6051
Preprint. Discussion started: 18 November 2026
© Author(s) 2026. CC BY 4.0 License.

episodes separated by less than 30 minutes into a single episode. Extreme HF air pressure episodes at Palagruža MB were identified using thresholds derived from the other MB stations.

We classified both HF sea level and HF air pressure extreme episodes into three intensity classes based on the maximum wave height and maximum NMV observed within each episode, using percentile thresholds [99.9–99.95) (hereafter $P_{99.9}$), [99.95–99.99) (hereafter $P_{99.95}$), [99.99–100] (hereafter $P_{99.99}$) of the corresponding distributions, to assess their mutual relationships and statistical properties. The corresponding thresholds and number of episodes are given in Tables 2 and 3. The number of HF sea level episodes per year is relatively consistent with previous studies (Ruić et al., 2023), yielding an average of 4 episodes annually for the two strongest classes. Station-specific wave-height thresholds of HF sea level extremes differ, as expected, due to local amplification effects related to bathymetry and coastal geometry (Monserrat et al., 2006). HF air pressure episodes outnumber HF sea level episodes because of their shorter duration, with relatively similar annual frequencies across MB stations, particularly for the strongest class, which occurs on average 5.5 times per year (Table 3).

Table 2. Extreme HF sea level episodes: percentile thresholds, number of HF sea level extreme episodes and yearly frequency, date, and wave height of the strongest HF sea level extreme episode.

Tide gauge	Wave-height class			Date of the strongest episode	Wave height [cm]
	$P_{99.9}$	$P_{99.95}$	$P_{99.99}$		
	Number of episodes / episodes per year				
Stari Grad	33.3 cm 20 / 2.7	38.4 cm 21 / 2.9	49.9 cm 10 / 1.4	9.7.2019	105.1
Vela Luka	38.8 cm 3 / 0.8	47.9 cm 8 / 2.1	69.8 cm 5 / 1.3	29.10.2018	94.1
Vis	31.5 cm 10 / 3	36.2 cm 7 / 2.1	46.6 cm 8 / 2.4	10.8.2021	61.5
Sobra	25.2 cm 15 / 2	28.5 cm 17 / 2.3	37 cm 8 / 1.1	10.1.2021	48.2
Bistrina	66.2 cm 7 / 2.2	75.6 cm 10 / 3.2	101.7 cm 3 / 1	22.7.2023	137.3

Table 3. Extreme HF air pressure episodes: percentile thresholds, number of HF air pressure extreme episodes, and yearly frequency, date, NMV, and maximum 5-minute rate of air pressure change of the strongest HF air pressure extreme episode.

Microbarograph	HF air pressure NMV class			Date of the strongest episode	NMV [hPa^2]	5-minute change [hPa]
	$P_{99.9}$ (~9.5 hPa^2)	$P_{99.95}$ (~14.7 hPa^2)	$P_{99.99}$ (~36 hPa^2)			
	Number of episodes / episodes per year					
Vrboska	75 / 11.4	81 / 12.3	35 / 5.3	21.10.2023	334.1	3.7
Vela Luka	86 / 11.9	87 / 12	46 / 6.4	22.7.2023	341.1	3.4
Vis	62 / 12	74 / 14.4	28 / 5.4	2.8.2019	165.9	2.6

https://doi.org/10.5194/egusphere-2026-6051
Preprint. Discussion started: 18 November 2026
© Author(s) 2026. CC BY 4.0 License.

Svetac	70 / 13.4	68 / 13.1	18 / 3.5	11.5.2020	169.2	2
Ražanj	68 / 13.9	73 / 15	21 / 4.3	19.8.2022	160.2	2.4
Ancona	36 / 11.5	50 / 16	27 / 8.6	30.8.2020	362.9	4.3
Ortona	112 / 16.7	101 / 15.1	35 / 5.2	10.7.2019	261.1	2.9
Vieste	56 / 14.7	43 / 11.1	21 / 5.4	24.7.2020	125.5	2.2

2.4 Connecting HF sea level and air pressure extreme episodes

We analysed the relationship between HF sea level and HF air pressure extreme episodes based on their co-occurrence by linking them in two directions. In the SL→AP direction, for each extracted extreme HF sea level episode we checked whether at least one HF air pressure episode at least at one MB station was recorded within a predefined period of interest. Conversely, in the AP→SL direction, for each extracted HF air pressure episode we checked whether at least one HF sea level extreme at least at one TG station was recorded within a corresponding period of interest. This window represents the largest plausible time interval within which an HF air pressure disturbance could propagate from a MB station to a TG station at which extreme HF sea level episode was recorded. For the purpose of defining these station-pair-specific windows, we assumed a minimum propagation speed of 10 m s^{-1} and considered atmospheric disturbances propagating from the south, southwest, west and northwest. No upper speed limit was imposed, as disturbances propagating faster than 10 m s^{-1} are inherently included within the defined propagation-time windows.

In the AP→SL direction, we defined the period of interest as a station-pair-specific time window around each HF air pressure episode, extending backward from the start of the episode and forward from its end (Table 4). The backward and forward extensions varied depending on the station pair and ranged from 3 hours before to 9.5 hours after the episode. In a few cases (restricted to Ortona and Vieste MBs), we shifted the beginning of the window forward relative to the start of the air pressure episode, by up to 1 hour, for station pairs where the expected propagation directions imply that atmospheric disturbances can only be detected before, and not after, the start of an HF sea level episode. These periods of interest thus account for both inter-station distance and the preferred propagation direction of atmospheric disturbances. The shortest periods of interest correspond to collocated stations, where the window extends from 1 hour before the start to 1 hour after the end of the HF air pressure episode.

Table 4. Periods of interest used to link HF air pressure and HF sea level extreme episodes for each MB–TG station pair. Time windows (in hours, h) are expressed relative to the start and end of HF air pressure episodes. Values in parentheses indicate the geographic distance (in km) between stations.

Micro-barograph	**Tide gauge**				
	Stari Grad	Vela Luka	Vis	Sobra	Bistrina
Vrboska	−1 h : +1 h (8 km)	−1 h : +1 h (25 km)	−1 h : +1 h (41 km)	−1.5 h : +3 h (92 km)	−1 h : +3 h (91 km)
Vela Luka	−1 h : +1 h (27 km)	−1 h : +1 h (0 km)	−1.5 h : +1 h (45 km)	−1 h : +2.5 h (78 km)	−1 h : +2.5 h (81 km)

https://doi.org/10.5194/egusphere-2026-6051
Preprint. Discussion started: 18 November 2026
© Author(s) 2026. CC BY 4.0 License.

Vis	−1 h : +1 h (34 km)	−1 h : +1.5 h (44 km)	−1 h : +1 h (<1 km)	−1 h : +3.5 h (122 km)	−1 h : +3.5 h (124 km)
Svetac	−1 h : +2 h (69 km)	−1 h : +2.5 h (78 km)	−1 h : +1 h (35 km)	−1 h : +4.5 h (155 km)	−1 h : +4.5 h (159 km)
Ražanj	−1 h : +1 h (21 km)	−1.5 h : +1.5 h (47 km)	−1 h : +1 h (34 km)	−2 h : +3.5 h (118 km)	−1.5 h : +3.5 h (116 km)
Palagruža	−1.5 h : +2.5 h (91 km)	−1 h : +2 h (74 km)	−1.5 h : +2.5 h (75 km)	0 h : +3.5 h (118 km)	0 h : +3.5 h (130 km)
Ancona	−1.5 h : +7 h (253 km)	−2 h : +7.5 h (270 km)	−2 h : +6 h (225 km)	−3 h : +9.5 h (348 km)	−2.5 h : +9.5 h (350 km)
Ortona	+1 h : +6 h (199 km)	+1 h : +5.5 h (200 km)	+1 h : +4.5 h (165 km)	+1 h : +7.5 h (266 km)	+1 h : +8 h (275 km)
Vieste	−2 h : +4 h (147 km)	−1.5 h : +3.5 h (127 km)	−2.5 h : +4 h (131 km)	+0.5 h : +4.5 h (152 km)	+0.5 h : +5 h (166 km)

We considered an HF air pressure episode associated with an HF sea level episode if the sea level episode occurred, at least partially, within the period of interest of HF air pressure episode. However, we imposed an additional condition that the overlap should occur within the first 90% of the sea level episode duration for MB stations in Croatia and within the first 80% for MB stations in Italy. If an air pressure episode (i.e., its period of interest) occurred during the last 10–20% of a sea level episode, we did not consider it associated, as the sea level episode was typically in its decaying phase.

In the opposite, SL→AP, direction we considered an HF sea level episode atmospherically forced if at least one HF air pressure episode occurred within the corresponding period of interest at any MB station. If multiple HF air pressure episodes were present, we associated all of them with the same sea level episode. We defined the SL→AP search window by applying the same logic used in the AP→SL direction, translating the forward extension applied after an air pressure episode into a backward extension before the sea level episode start. For example, a 2-hour forward extension after the end of an air pressure episode corresponds to a 2-hour backward extension before the start of the sea level episode. We then searched for HF air pressure extremes from this extended start time until 90% (for MBs in Croatia) or 80% (for MBs in Italy) of the sea level episode duration. This approach ensures consistent coupling intervals in both directions and considers only the first 80–90% of each sea level episode.

2.5 Analysis of connected HF sea level and air pressure episodes

After establishing matched episode pairs, we performed analyses on the connected episodes. We compared the intensities of HF sea level and HF air pressure episodes across all available station pairs. In the SL→AP direction, we examined the relationship between sea level and atmospheric pressure intensity by identifying the maximum NMV within a window extending backward (according to the period-of-interest definition) from the start of each sea level episode to up to 2.5 hours after the time of maximum sea level wave height, depending on the station pair. In the AP→SL direction, we repeated the same procedure, but with the period-of-interest windows defined around HF air pressure episodes according to Table 4.

https://doi.org/10.5194/egusphere-2026-6051
Preprint. Discussion started: 18 November 2026
© Author(s) 2026. CC BY 4.0 License.

To identify the typical propagation speed and direction of atmospheric disturbances forcing the extreme sea level episodes, we estimated the median time lag between the peak wave height of each sea level episode at each TG and the nearest point in the HF air pressure NMV series exceeding the 99.9th percentile at each MB station for the connected episodes, using the same search window as defined for the maximum NMV in the SL→AP direction. Given the high spatial and temporal changeability of atmospheric pressure disturbances, we cannot claim with certainty that, while tracking the nearest extreme NMV across the network, we are tracking the same individual atmospheric disturbance, and that the estimated propagation velocity of the nearest extreme NMV translates directly to propagation velocity of the atmospheric disturbances which caused HF sea level extremes. The estimated velocities should therefore be considered with caution. We then spatially interpolated the resulting median time lags using Gaussian process regression (Rasmussen and Williams, 2005) with an exponential kernel function across the domain bounded by the available MBs to map the typical propagation patterns. To calculate the corresponding propagation speed and direction from the median time-lag field, we used an isochronal analysis method (Thomson et al., 2009), which assumes that air pressure disturbances propagate as plane waves with a constant speed and direction. For the isochronal analysis, the Vis MB was excluded because of the temporal drift in its recorded time series, as described in Sect. 2.1.

We further analysed the simultaneity of HF sea level and HF air pressure episodes across stations to evaluate the spatial coherence of HF oscillations. ERA5 global reanalysis data (Hersbach et al., 2020) were used in Discussion to place selected episodes in a broader synoptic context and to assess whether large-scale atmospheric conditions were favourable for their occurrence.

3 Results

3.1 General statistics of HF extremes

The episode statistics derived from the HF sea level series for the three intensity classes ($P_{99.9}$, $P_{99.95}$, $P_{99.99}$ wave-height thresholds) are summarised in Table 2. Considerable differences among stations reflect the strong influence of local amplification processes. Bistrina exhibits substantially larger thresholds than all other TGs, with wave-height thresholds reaching 66.2 cm, 75.6 cm and 101.7 cm for the 99.9th, 99.95th and 99.99th percentiles, respectively. Stari Grad and Vis TGs record similar extreme thresholds across all three classes (~30–50 cm), with Vela Luka TG having slightly higher thresholds (up to 70 cm). The strongest HF sea level episode at each station is also highly variable, with Bistrina TG recording the largest episode in the dataset on 22 July 2023 (137.3 cm trough-to-crest). Other station maxima include Stari Grad TG (105.1 cm on 9 July 2019), Vela Luka TG (94.1 cm on 29 October 2018), Vis TG (61.5 cm on 10 August 2021), and Sobra TG (48.2 cm on 10 January 2021). Sobra TG represents a special case among the analysed stations. It exhibits relatively modest extreme wave heights, thereby having the lowest percentile thresholds in the dataset (up to 37 cm). Visual inspection of the Sobra sea level records reveals that considerable short-period (2–5 minutes) oscillations are present almost continuously, particularly during the colder part of the year. It should be noted here that at some of herein studied locations considerably higher HF sea level extremes were observed prior to the installation of TGs and/or at the head of the bays (TGs are not installed at head of the

https://doi.org/10.5194/egusphere-2026-6051
Preprint. Discussion started: 18 November 2026
© Author(s) 2026. CC BY 4.0 License.

bays, but commonly closer to the middle of the bays). The strongest known HF event in Vela Luka, the Great Vela Luka meteotsunami of 21 June 1978 had a wave height of ~6 meters at the top of the bay, and the strongest known Stari Grad event (23 June 2003) had a height of ~3.5 meters, also at the top of the bay (Vilibić et al., 2004; Orlić, 2015). Thus, if we had longer sea level time series and TGs closer to the head of the bay, the statistics would likely be different and more in line with the historic observations.

The statistics of extreme HF air pressure episodes, also grouped into three percentile-based intensity classes, are summarised in Table 3. Unlike sea level, whose thresholds vary substantially among TG stations due to local bathymetry effects, air pressure thresholds are identical throughout the network, as explained in Sect. 2.2, due to general properties of HF atmospheric pressure series and spatially coherent atmospheric HF variability over the middle Adriatic. The thresholds corresponding to the 99.9th, 99.95th, and 99.99th percentiles are ~9.5 hPa^2, ~14.7 hPa^2, and ~36 hPa^2, respectively, corresponding to, at the most, ~0.85 hPa, ~1 hPa, and ~1.6 hPa 5-minute rate of air pressure change. HF air pressure episodes occur considerably more frequently than HF sea level episodes, ranging from 29 episodes per year at Vrboska MB to 37 episodes per year at Ortona MB.

The strongest HF air pressure episode in the dataset was recorded at Ancona MB on 30 August 2020, reaching an NMV of 362.9 hPa^2 and a rate of air pressure change of 4.3 hPa over 5 minutes. Comparable atmospheric disturbances were observed at other stations as well. The weakest among the station-wise maxima occurred at Vis MB on 2 August 2019, where a 2.6 hPa change over 5 minutes was recorded, corresponding to an NMV of 165.9 hPa^2. We found only one co-occurrence of the strongest HF air pressure episode and the strongest HF sea level episode: the strongest air pressure episode at Vela Luka MB (recorded on 22 July 2023) coincided with the strongest HF sea level episode at Bistrina TG.

3.2 Extreme HF sea level episode connections with extreme HF air pressure episodes

Extreme HF sea level episodes were generally accompanied by at least one recorded HF air pressure extreme. Figure 4 illustrates a representative example from Stari Grad TG on 22–23 July 2023. During this HF sea level episode, several nearby MB stations (Vrboska, Vela Luka, Svetac) recorded an extreme HF air pressure disturbance within the period of interest associated with the sea level extreme. More distant MBs (Palagruža and Ortona) did not record any extreme atmospheric disturbances.

Table 5 reveals high overall connection rates between SL and AP episodes, reaching 96% at Stari Grad TG (49 of 51 episodes), 100% at Vela Luka TG (16 of 16 episodes), 92% at Vis TG (23 of 25 episodes), 95% at Sobra TG (38 of 40 episodes), and 80% at Bistrina TG (16 of 20 episodes). Thus, the vast majority of extreme sea level episodes coincide with at least one HF air pressure extreme recorded within the network. Connection rates with individual MB stations are also generally high, although they vary among station pairs. The strongest station-pair connections are found between Stari Grad TG and Ortona MB (89%), Vela Luka TG and MB (88%), Vela Luka TG and Vis MB (87%), Vela Luka TG and Ortona MB (85%), and Bistrina TG and Ražanj MB (89%). High connection rates are observed for station pairs spanning both the eastern and western Adriatic, indicating that the atmospheric disturbances are often detected over large spatial scales during HF sea level extremes.

https://doi.org/10.5194/egusphere-2026-6051
Preprint. Discussion started: 18 November 2026
© Author(s) 2026. CC BY 4.0 License.

However, we note that in some cases, and especially in those where an associated atmospheric pressure extreme was detected only at an MB station in Italy, the available observations do not allow the identified pressure disturbance to be confirmed unequivocally as the direct cause of the corresponding sea level episode. Although these episodes are included in the statistical connection, they provide only evidence that significant atmospheric activity occurred during the relevant period. Despite its favourable location for capturing propagating atmospheric disturbances, Palagruža MB exhibits the lowest average connection rate with the TG stations (65%), but this can also reflect numerous issues with Palagruža MB data.

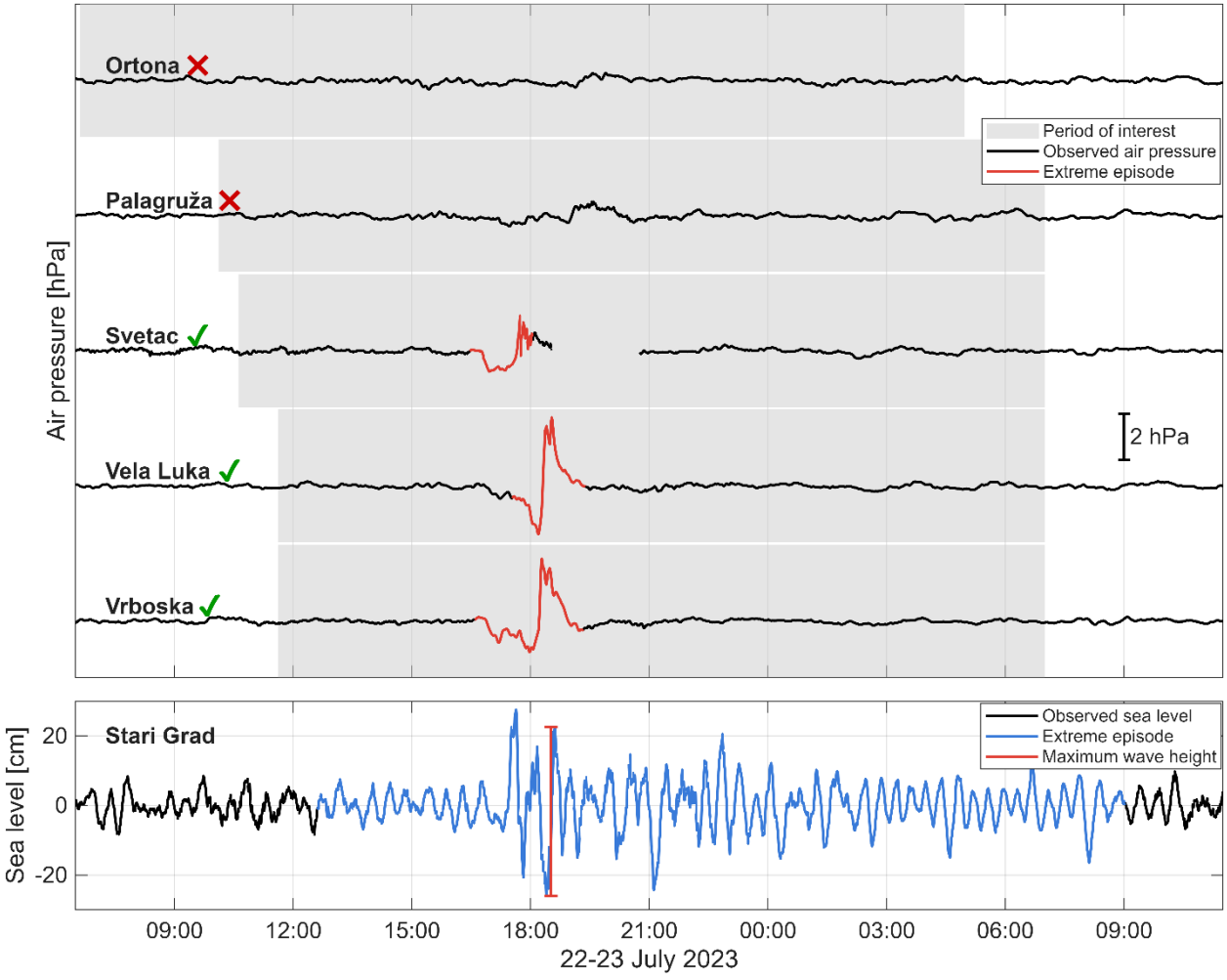


Figure 4. An example of a sea level extreme at Stari Grad TG and its connection to air pressure episodes at five middle Adriatic MB stations. The MBs without available measurements at the time are not shown. Time is given in UTC.

Table 5. Percentage of sea level extremes at each TG that are connected to air pressure extremes at individual MB stations. Values in parentheses indicate the overall number of sea level extremes with available air pressure data. The Overall column shows the total connection across all MB stations. Dashes (–) indicate cases with no simultaneous measurements. Highest station-pair connections are bolded. VRB stands for Vrboska, VL for Vela Luka, VIS for Vis, SVE for Svetac, RAŽ for Ražanj, PAL for Palagruža, ANC for Ancona, ORT for Ortona, VIE for Vieste.

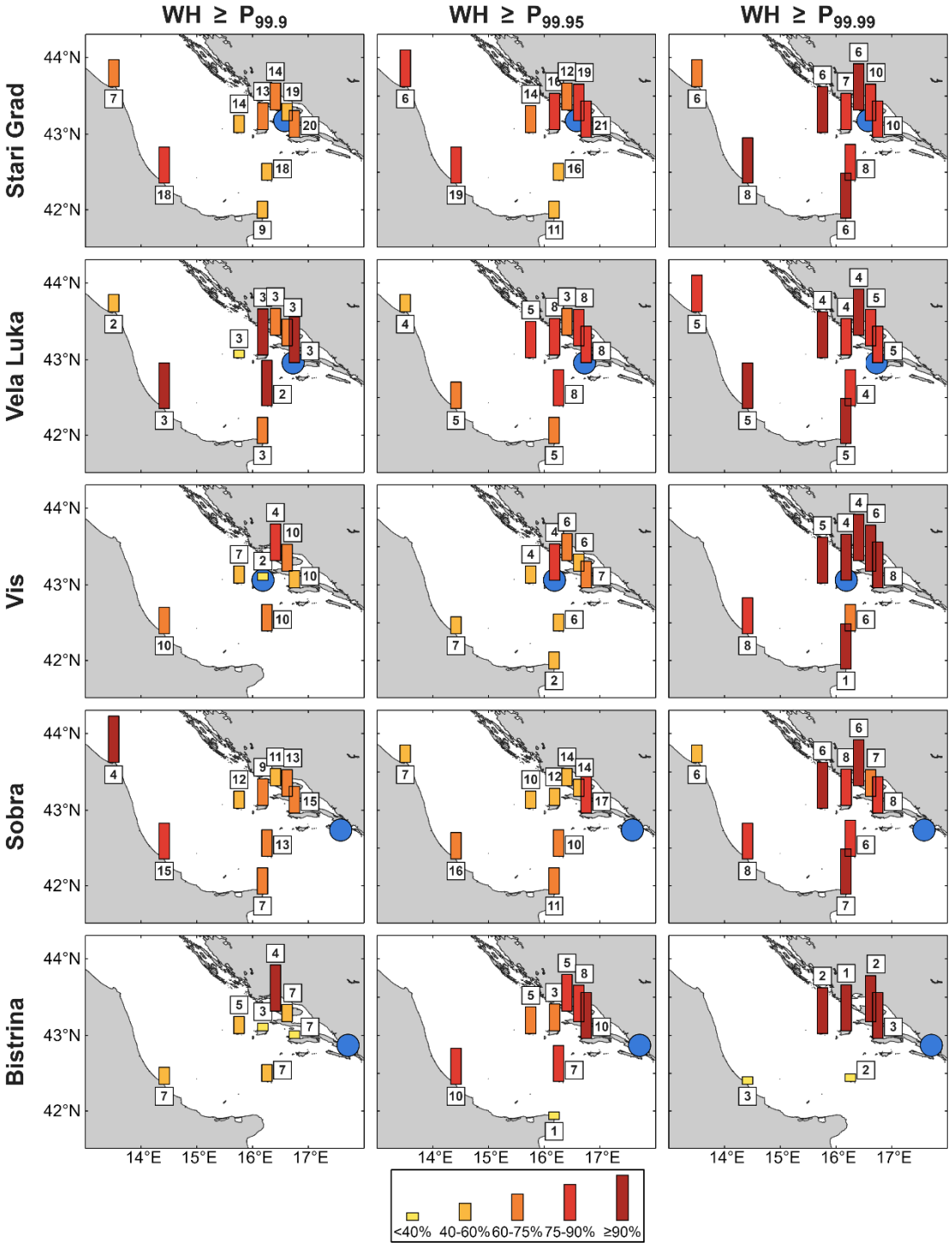
https://doi.org/10.5194/egusphere-2026-6051
Preprint. Discussion started: 18 November 2026
© Author(s) 2026. CC BY 4.0 License.

Tide gauge	Microbarograph									Overall
	VRB	VL	VIS	SVE	RAŽ	PAL	ANC	ORT	VIE	
Stari Grad	71 % (48)	73 % (51)	75 % (36)	68 % (34)	72 % (32)	62 % (42)	74 % (19)	**89 %** (45)	62 % (26)	96 % (51)
Vela Luka	81 % (16)	**88 %** (16)	87 % (15)	75 % (12)	80 % (10)	79 % (14)	64 % (11)	85 % (13)	77 % (13)	100 % (16)
Vis	68 % (22)	72 % (25)	70 % (10)	63 % (16)	**79 %** (14)	59 % (22)	–	68 % (25)	67 % (3)	92 % (25)
Sobra	62 % (34)	75 % (40)	66 % (29)	61 % (28)	61 % (31)	69 % (29)	65 % (17)	**77 %** (39)	76 % (25)	95 % (40)
Bistrina	76 % (17)	70 % (20)	57 % (7)	58 % (12)	**89 %** (9)	56 % (16)	–	65 % (20)	0 % (1)	80 % (20)

To examine how connection rates vary with sea level intensity, we mapped the percentage of sea level extremes that are connected to HF air pressure extremes at individual MB stations, separately for the three wave-height intensity classes (Fig. 5). A consistent pattern emerges across all TGs – connection rates generally increase with wave-height percentile.

At Stari Grad TG, connection rates in the $P_{99.9}$ class range from 44% (Vieste MB) to 83% (Ortona MB), based on 7–20 episodes per station. They increase in higher percentile classes and reach up to 100% at several stations in the $P_{99.99}$ class. At Vela Luka TG, connection rates in the $P_{99.9}$ class vary between 33% (Svetac MB) and 100% (Ortona, Palagruža, Vis, Vela Luka MBs), although these estimates are based on only 2–3 episodes per station. The $P_{99.99}$ class shows uniformly high values, with several stations reaching 100% but still based on limited sample sizes (4–5 episodes). Vis TG shows moderate connection rates in the $P_{99.9}$ class, with most stations ranging from 50% to 75%. Only with Vis MB connection rate is 0% (based on 2 episodes). Connection rates for Vis TG generally increase in higher percentile classes, up to 100%. At Sobra TG, connection rates in the $P_{99.9}$ class range from 55% to 100% (4–15 episodes per station) and increase consistently with percentile class, with Ortona and Vela Luka MBs among the most frequently connected stations. Bistrina TG shows the largest variability, from 29% (Vela Luka MB) to 100% (Ražanj MB) in the $P_{99.9}$ class. In the $P_{99.99}$ class, connection rates are higher, but many values are based on very small sample sizes (1–3 episodes). For the $P_{99.99}$ class, all TGs show a 100% connection with at least one MB station.

https://doi.org/10.5194/egusphere-2026-6051
Preprint. Discussion started: 18 November 2026
© Author(s) 2026. CC BY 4.0 License.



405 **Figure 5.** Spatial distribution of connection rates between sea level extremes at each TG (blue circle) and HF air pressure extremes at individual MB stations (bars), shown separately for three wave-height percentile classes ($P_{99.9}$, $P_{99.95}$, $P_{99.99}$). Shading indicates the connection rate (fraction of connected episodes relative to the total number of sea level extremes for which there is available air pressure data at a given

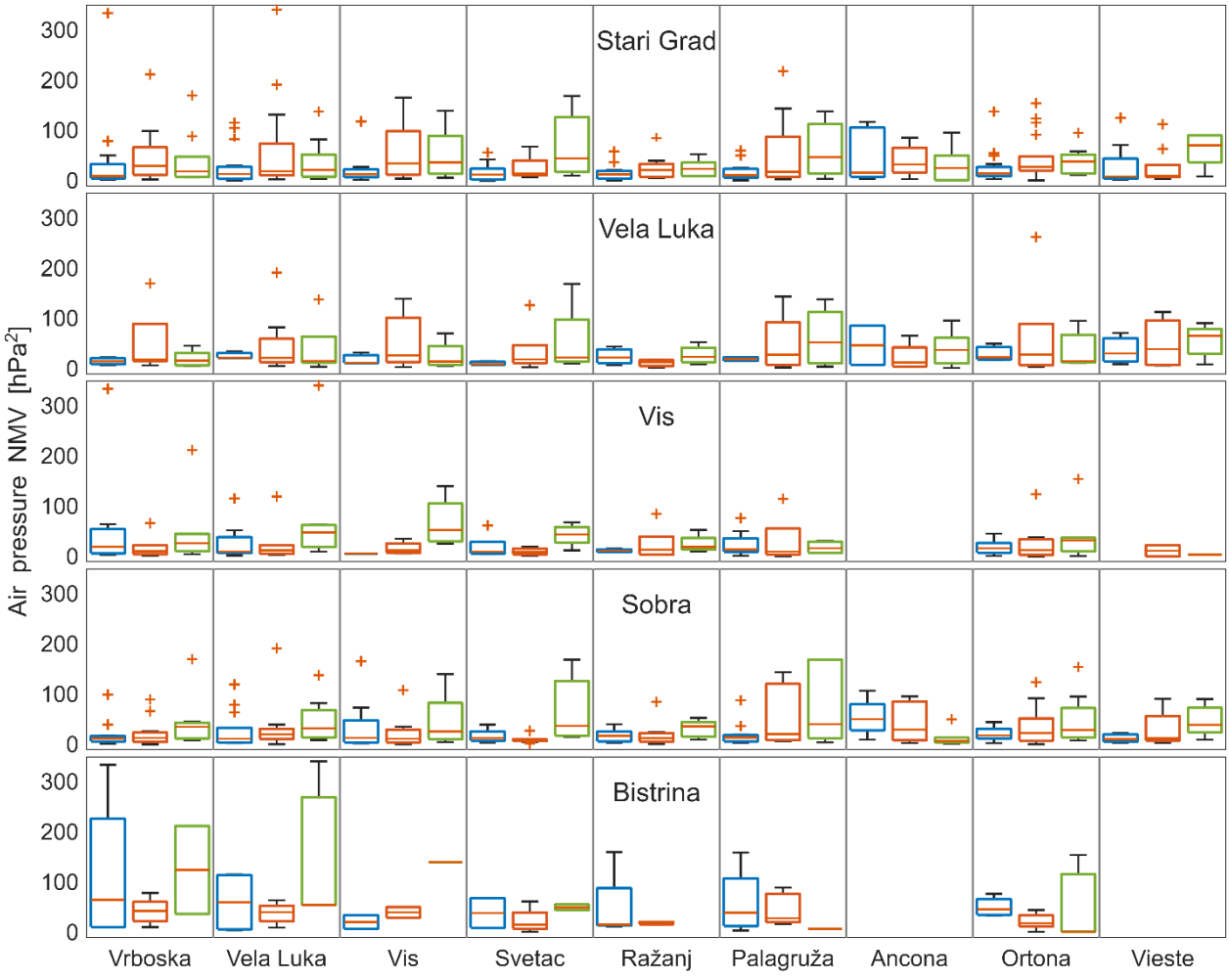
https://doi.org/10.5194/egusphere-2026-6051
Preprint. Discussion started: 18 November 2026
© Author(s) 2026. CC BY 4.0 License.

MB) for each TG–MB pair. The numbers in white boxes indicate the total number of sea level episodes in that class for which concurrent air pressure measurements were available.

3.3 HF air pressure intensity across wave-height intensity classes

For connected episodes, we analysed the maximum HF air pressure NMV, which potentially contributed to the peak wave height. Figure 6 shows the distribution of these maximum NMV values grouped by wave-height percentile class for each TG–MB pair. Across all TGs, the median value of NMV maxima generally increases with wave-height percentile, indicating that stronger sea level oscillations tend to be associated with more intense atmospheric forcing, especially at Stari Grad and Sobra TGs, where the median NMV for the highest wave-height class typically reaches 20–50 hPa^2, compared to the typical 10–20 hPa^2 for the lowest class. However, the interquartile ranges overlap substantially between wave-height classes at most TG–MB pairs, indicating that the class median alone cannot fully account for the atmospheric forcing responsible for an individual peak wave height; occasional high NMV outliers are present even within the lowest wave-height class. Vela Luka TG deviates somewhat from this pattern, as for 5 out of 9 MB stations the median NMV in the lowest or intermediate class exceeds that of the highest wave-height class. Bistrina TG shows fewer extreme sea level episodes, so the statistics are less reliable due to the limited sample size. Occasionally, e.g., for the Sobra TG–Ancona MB and Bistrina TG–Ortona MB station pairs, we observe the opposite pattern, with median atmospheric forcing decreasing as the wave-height class increases – likely reflecting the relatively low connection rates in the $P_{99.99}$ wave-height class for these pairs (shown in Fig. 5).

https://doi.org/10.5194/egusphere-2026-6051
Preprint. Discussion started: 18 November 2026
© Author(s) 2026. CC BY 4.0 License.



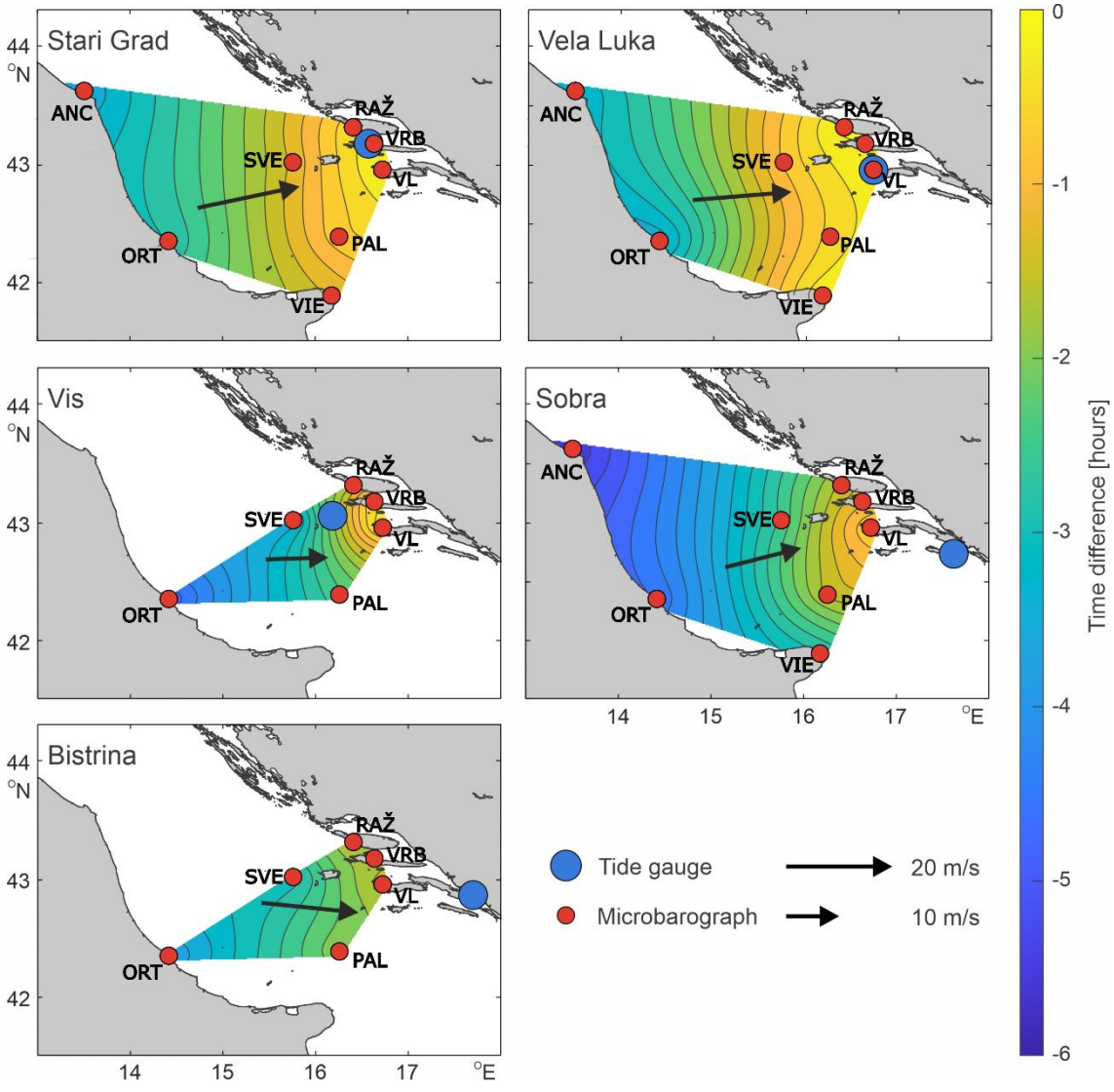
425 **Figure 6.** Box plots of the maximum HF air pressure NMV associated with each sea level extreme, grouped by HF sea level wave-height percentile class (blue: $P_{99.9}$, orange: $P_{99.95}$, green: $P_{99.99}$).

3.4 Propagation speeds and directions of atmospheric disturbances

The median time-lag fields (Fig. 7) reveal consistent propagation patterns across all five TGs. It should be noted here once again that although the time lags between maximum wave height and closest extreme NMV do not necessarily "catch" the
430 atmospheric disturbance responsible for HF extreme, the median time-lag fields do provide a useful first guess. Proper identification of corresponding HF atmospheric and sea level extremes would require careful consideration of time series of both HF sea level and air pressure components – which is a topic which we plan to further pursue. Meanwhile, according to velocity estimated based on median time-lag fields, atmospheric disturbances associated with the observed sea level extremes generally propagate from westerly directions, with estimated typical propagation speeds ranging between 12 and 20 m s^{-1},
435 depending on the tide gauge. For Stari Grad TG, the atmospheric disturbances typically propagate from the west-southwest (γ = 257.6°) at a median speed of 19.9 m s^{-1}, while for Vela Luka TG they propagate from the west (γ = 263.3°) at 18.1 m s^{-1}. In

https://doi.org/10.5194/egusphere-2026-6051
Preprint. Discussion started: 18 November 2026
© Author(s) 2026. CC BY 4.0 License.

both cases, the largest time lags occur at the westernmost stations, reaching approximately 3.5 hours, whereas the sea level response is nearly simultaneous with the atmospheric disturbance at the closest stations. Vis TG exhibits a distinct pattern compared with Stari Grad and Vela Luka TGs, with a considerably larger time difference between the arrival of the atmospheric disturbance and the corresponding sea level response at the collocated MB and TG (~100 minutes, compared with <4 minutes at Vela Luka). The estimated propagation speed is lower (11.8 m s^{-1}), with atmospheric disturbances propagating from the west (γ = 266.3°). For Sobra TG, disturbances typically propagate from the west-southwest (γ = 256.3°) at a median speed of 14.6 m s^{-1}. Similarly, for Bistrina TG, the atmospheric disturbances typically propagate from the west (γ = 277°) at a median speed of 19.8 m s^{-1}. The largest time lags reach approximately 4.5 hours for Vis, 5.5 hours for Sobra and 3.7 hours for Bistrina TG.



https://doi.org/10.5194/egusphere-2026-6051
Preprint. Discussion started: 18 November 2026
© Author(s) 2026. CC BY 4.0 License.

Figure 7. Median time-lag field, interpolated from microbarograph station data, between peak wave heights of sea level extremes and the nearest associated extreme HF air pressure NMV. We excluded MB stations contributing fewer than four episodes for a given TG, as they are considered insufficiently representative. Vis MB was also excluded due to the temporal drift in the recorded time series.

3.5 Extreme HF air pressure episode connections with extreme HF sea level episodes

Figure 8 illustrates a representative example associated with an extreme HF air pressure episode recorded at the Vrboska MB on 4–5 August 2023. During this episode, Stari Grad and Vis TGs recorded extreme HF sea level oscillations. Bistrina TG experienced the largest wave heights; however, these remained below the station-specific extreme threshold (with wave heights corresponding to ~99.83rd percentile of wave heights), consistent with the relatively high percentile threshold adopted for this station (Table 2). Sobra TG also recorded pronounced HF sea level oscillations following the atmospheric disturbance (with wave heights corresponding to ~99.45th percentile of wave heights), although they did not exceed the extreme 99.9th percentile threshold.

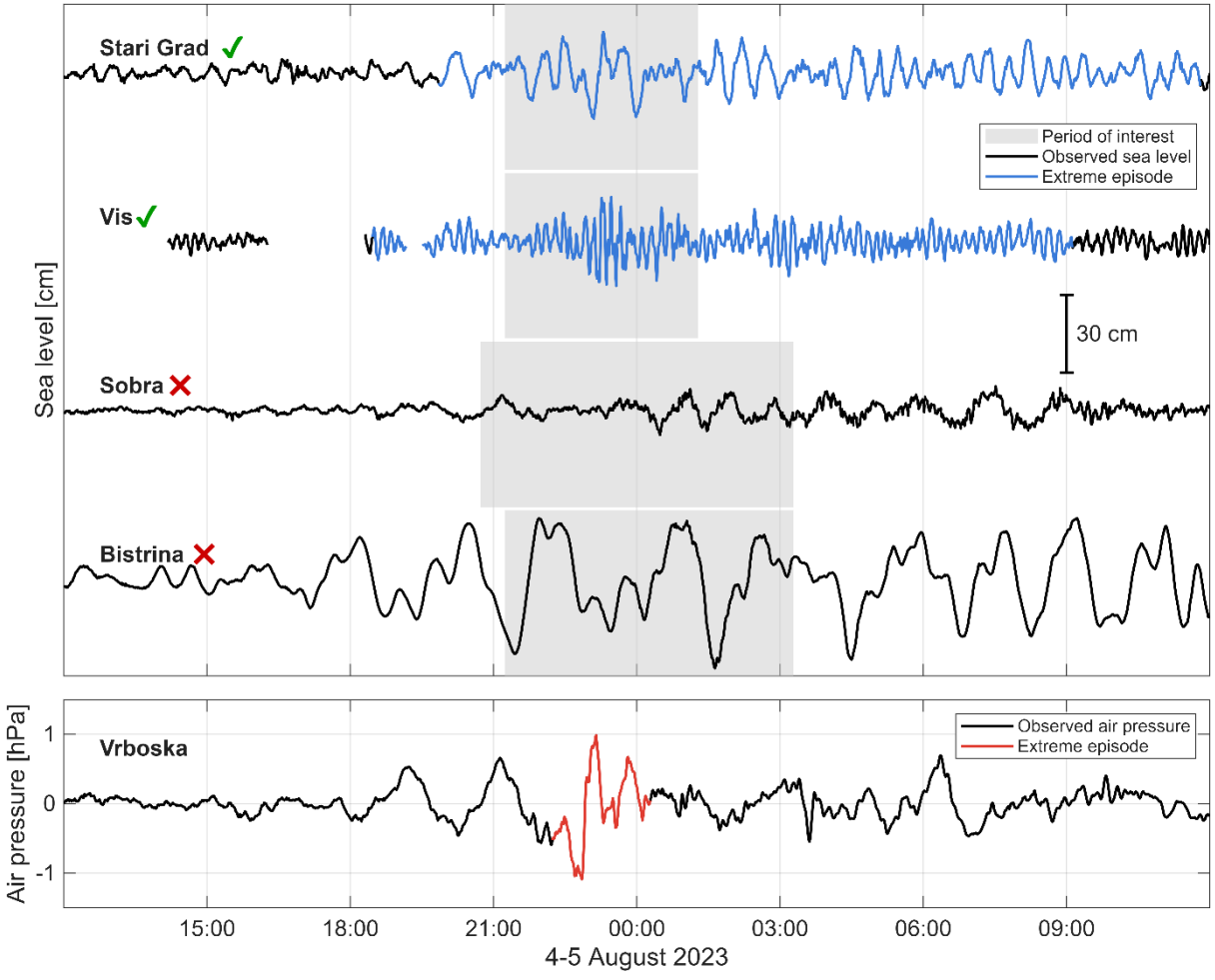


Figure 8. An example of an air pressure extreme at Vrboska MB and its connection to sea level extremes at numerous TG stations. Time is given in UTC.

https://doi.org/10.5194/egusphere-2026-6051
Preprint. Discussion started: 18 November 2026
© Author(s) 2026. CC BY 4.0 License.

The results of the AP→SL connection analysis are summarised in Table 6. Overall connection rates are considerably lower than those obtained in the SL→AP analysis, ranging from 32% for Ancona to 45% for Vela Luka MB. Individual connection rates generally range between 13% and 32%. The strongest station-pair connections are observed between the Vrboska, Vela Luka and Vis MBs with TGs at Stari Grad and Vis (30–32%). All MB stations exhibit comparable overall connection rates, ranging from 32% to 45%. Vela Luka, Vieste, Vrboska, Ortona, and Vis MBs show the highest overall connection rates (38–45%), whereas Svetac, Ražanj, and Ancona MBs show somewhat lower values (32–35%).

Table 6. Percentage of air pressure extremes at each MB that are connected to sea level extremes at individual TGs. Values in parentheses indicate the overall number of air pressure extremes for which sea level data were available sea level. The Overall column shows the overall connection across all TGs. Dashes (–) indicate cases with no simultaneous measurements. Highest station-pair connections are bolded.

Microbarograph	Tide gauge					Overall
	Stari Grad	Vela Luka	Vis	Sobra	Bistrina	
Vrboska	**31%** (188)	25% (106)	30% (83)	20% (187)	24% (75)	40% (191)
Vela Luka	**32%** (216)	23% (110)	**32%** (106)	24% (215)	22% (95)	45% (219)
Vis	31% (160)	21% (122)	**32%** (38)	19% (163)	21% (28)	38% (164)
Svetac	22% (156)	18% (90)	**26%** (65)	17% (156)	18% (60)	34% (156)
Ražanj	22% (162)	14% (89)	**26%** (72)	17% (156)	22% (59)	35% (162)
Ancona	**26%** (113)	16% (109)	–	17% (113)	–	32% (113)
Ortona	**29%** (248)	19% (142)	26% (104)	20% (245)	20% (98)	39% (248)
Vieste	28% (120)	23% (106)	23% (13)	**30%** (120)	0% (7)	41% (120)

Figure 9 shows how episode connections vary with air pressure percentile class at mid-distance stations (located in Croatia), while Fig. 10 presents the same for long-distance stations (located in Italy). Again, we see a clear tendency of increasing connection with air pressure intensity, showing a stronger and more coherent coupling during the most extreme atmospheric disturbances. For the $P_{99.9}$ class, connection rates are generally low to moderate, typically ranging between 10% and 30% across most station pairs. In the $P_{99.95}$ class, connection percentages increase slightly for most station pairs, with several exceeding ~30%. The strongest and most coherent patterns emerge in the $P_{99.99}$ class, where connection rates increase substantially across nearly all station pairs. Many station pairs exceed 50% and, in several cases, exceed 60–70%, particularly those involving Vrboska, Vela Luka, Svetac, and Vieste MBs. In this class, connection percentages with at least one TG station reach 71.4% for Vrboska, 67.4% for Vela Luka, 53.6% for Vis, 50.0% for Svetac, 61.9% for Ražanj, 51.9% for Ancona, 65.7% for Ortona, and 76.2% for Vieste MB.

https://doi.org/10.5194/egusphere-2026-6051
Preprint. Discussion started: 18 November 2026
© Author(s) 2026. CC BY 4.0 License.

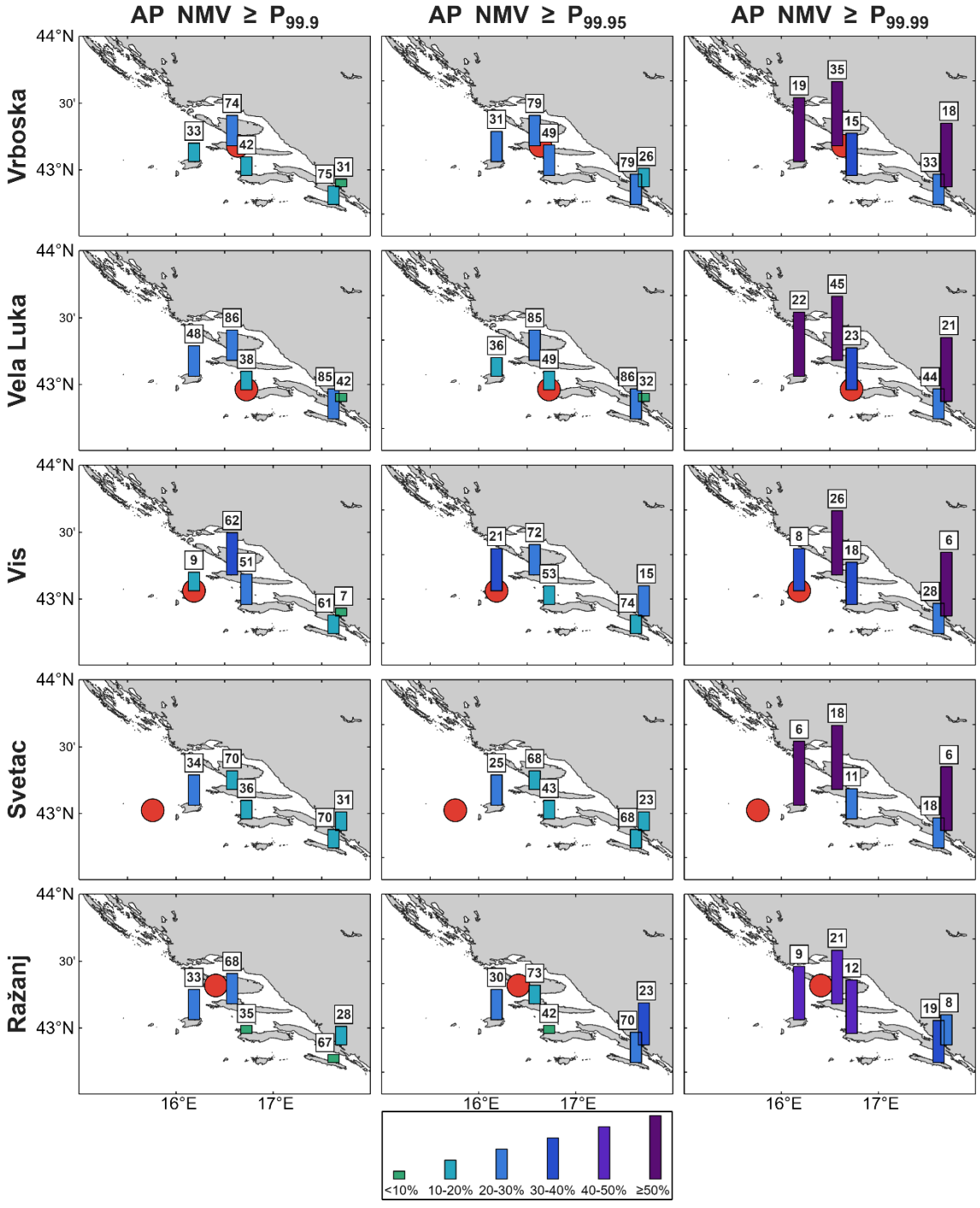


Figure 9. Spatial distribution of connection rates between HF air pressure extremes at each MB and HF sea level extremes at individual TG stations for mid-distance stations, shown separately for three air pressure percentile classes ($P_{99.9}$, $P_{99.95}$, $P_{99.99}$). Shading indicates the connection rate (fraction of connected episodes relative to the total number of air pressure extremes with available sea level data) for each MB–TG pair. The numbers in white boxes indicate the total number of air pressure episodes in that class for which concurrent sea level measurements were available.

https://doi.org/10.5194/egusphere-2026-6051
Preprint. Discussion started: 18 November 2026
© Author(s) 2026. CC BY 4.0 License.

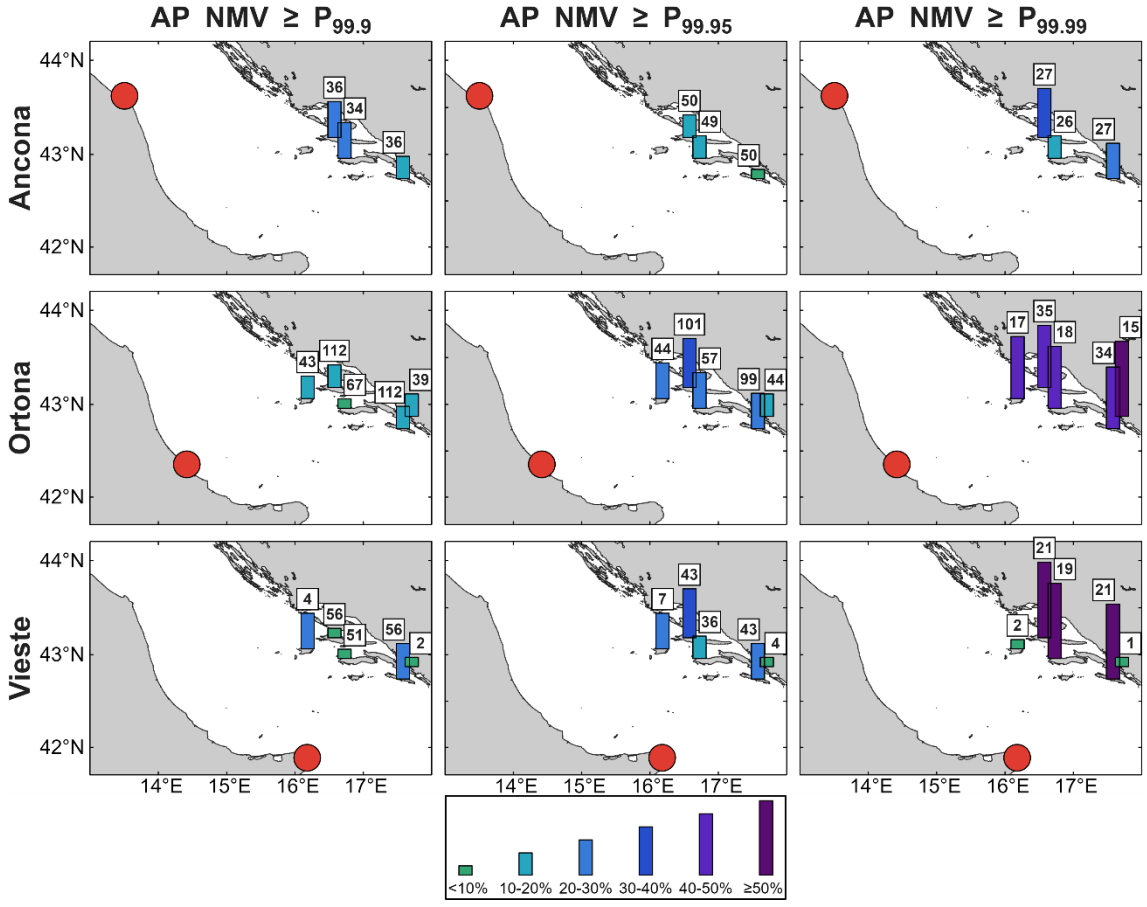


Figure 10. Same as Fig. 9, but for long-distance MB stations.

3.6 HF sea level intensity across HF air pressure NMV intensity classes

To further examine the sea level response associated with extreme HF air pressure episodes, we analysed the maximum wave height at each TG within the corresponding periods of interest defined in Table 4. Figure 11 presents box plots of these maximum wave heights grouped by air pressure intensity class for each MB–TG pair. Across most MB and TG combinations, median wave height increases with stronger air pressure intensity class, indicating that stronger atmospheric disturbances are generally associated with higher HF sea level oscillations. This trend is most pronounced for Bistrina TG, where median wave heights increase substantially between intensity classes, reaching 95 cm in the strongest class compared with 40 cm in the weakest class for Svetac MB–Bistrina TG pair. As in the reverse analysis (Fig. 6), the interquartile ranges overlap considerably between classes at most MB–TG pairs, indicating that air pressure intensity class alone does not determine the HF sea level wave height within an individual episode. Sobra TG shows weaker differences between classes, with median wave heights remaining low (15–30 cm). Several station pairs deviate from the overall trend, with the intermediate or the weakest class occasionally exhibiting higher median HF sea level wave heights than the strongest class.

https://doi.org/10.5194/egusphere-2026-6051
Preprint. Discussion started: 18 November 2026
© Author(s) 2026. CC BY 4.0 License.

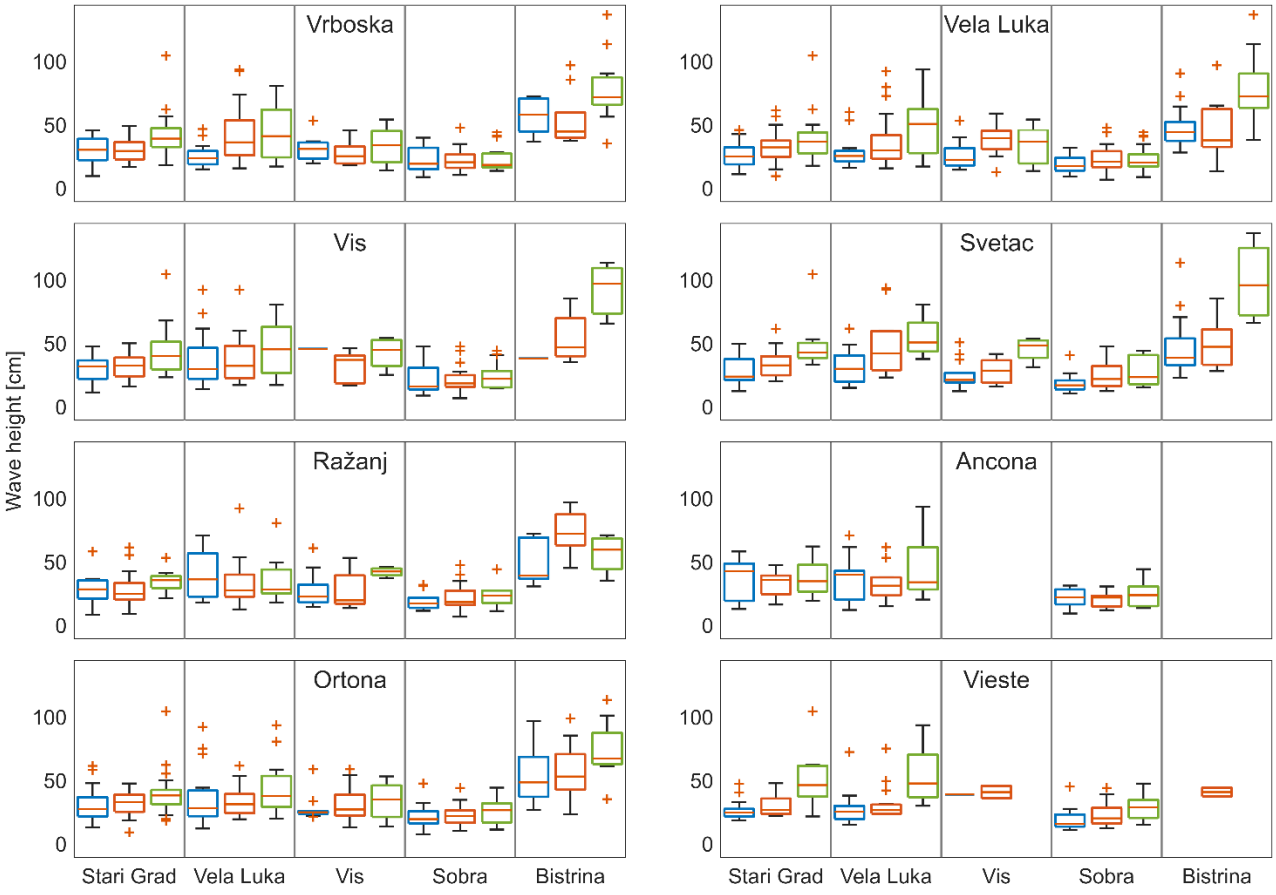


Figure 11. Box plots of the maximum wave heights associated with each air pressure extreme, grouped by air pressure percentile class (blue: $P_{99.9}$, orange: $P_{99.95}$, green: $P_{99.99}$).

4 Discussion

This study provides a first statistical assessment of the relationship between extreme HF sea level and HF atmospheric pressure episodes across the regional monitoring network located in the middle Adriatic. The analysis is not intended to resolve the detailed characteristics or generation mechanisms of individual episodes, but rather to identify their statistical relationship. Due to the lack of sufficiently long, simultaneous high-resolution sea level and atmospheric pressure observations, such an analysis was previously not done at the regional scale at any World location. Our study, which is based on data from an observational network that was initially envisioned precisely to track meteotsunamis, thus presents a first of its kind.

The conducted research points that there is a strong statistically credible association between HF atmospheric pressure extremes and HF sea level extremes over the middle Adriatic (Table 5). Our main finding is the following: most of the HF sea level extremes were associated with at least one HF air pressure extreme (only 7 out of total of 85 sea level episodes are not

https://doi.org/10.5194/egusphere-2026-6051
Preprint. Discussion started: 18 November 2026
© Author(s) 2026. CC BY 4.0 License.

associated with any HF air pressure extreme), whereas substantially smaller percentage, i.e., 32–45% of HF air pressure extremes were associated with at least one HF sea level extreme, depending on the microbarograph.

The association of HF sea level extremes to HF air pressure disturbances was more robust for stronger sea level episodes (Fig. 5), reaching complete association for the most extreme class ($P_{99.99}$) for all TG stations. It is important to note that connection rates were similar for mid- and long-distance MB-TG station pairs – clearly indicating that atmospheric pressure disturbances responsible for onset of HF sea level oscillations can propagate from the western towards the eastern Adriatic coast across distances of up to 350 km (Table 4). This finding also implies that both nearby and distant atmospheric measurements can be used as an observational basis for real-time tracking and forecasting of HF sea level extremes, including meteotsunamis.

Although stronger atmospheric pressure disturbances are generally associated with stronger sea level episodes, there is a substantial overlap between atmospheric pressure and sea level intensity classes (Fig. 6), implying that atmospheric pressure intensity alone is not sufficient to explain the magnitude of the sea level response. It is known that efficient transfer of atmospheric energy to the ocean requires favourable resonance conditions. In both Proudman (Proudman, 1929) and Greenspan (Greenspan, 1956) resonances, the energy transfer is highly sensitive to the relationship between the propagation speed of the atmospheric disturbance and the speed of the long ocean waves (Vilibić, 2008), with departures from fully resonant conditions rapidly reducing the long ocean wave growth (Vilibić, 2008). Thus, if propagating with a speed close to resonant one, a weak HF atmospheric pressure disturbance can generate strong HF sea level oscillations, whereas, if propagating with a speed that strongly differs from a resonant one, a strong HF atmospheric pressure disturbance can result only with weak HF sea level oscillations.

To account for propagation velocity of atmospheric disturbances, we have inferred typical propagation directions and speeds of specific characteristics of those atmospheric disturbances which were associated with extreme HF sea level episodes (Fig. 7). According to our analysis these atmospheric disturbances were predominantly coming from the west, consistent with directions of atmospheric disturbances which caused some of the strongest studied Adriatic Sea meteotsunamis (e.g., Vilibić et al., 2004; Šepić et al., 2009; Orlić et al., 2010; Šepić et al., 2016), and their propagation speeds, estimated from median time between detection of a specific feature of atmospheric disturbance and the highest sea level oscillation, were 12 to 20 m s^{-1}, depending on the tide gauge. Such propagation directions and speeds favour occurrence of strong HF sea level extremes along westward-facing coasts and over depths of ~15 to 40 meters. Most of our stations face west, and sea depths of the specified range can indeed be found on pathways of atmospheric disturbances which propagate towards these stations.

It should be noted that significant HF sea level oscillations have also been observed at the Adriatic Sea locations that do not directly face these directions, including Vis and Sobra TGs (analysed in this paper), but also Široka Bay (Ist Island) and Vrboska (Šepić et al., 2009; Tojčić et al., 2021; Ruić et al., 2023; Šepić and Orlić, 2026), indicating that direct exposure to the incoming atmospheric disturbance is not a prerequisite for a strong coastal response. In our study, this is evident at Vis TG, where the inferred atmospheric disturbances likely propagate from the west (Fig. 7), whereas the harbour entrance faces north-northeast. Meteotsunami generation is generally expected to be more efficient when the harbour opening is oriented towards the approaching disturbance, allowing direct inflow of long ocean waves generated over open sea by resonant atmospheric

https://doi.org/10.5194/egusphere-2026-6051
Preprint. Discussion started: 18 November 2026
© Author(s) 2026. CC BY 4.0 License.

forcing (Vilibić et al., 2025). Nevertheless, significant HF oscillations are frequently observed at Vis TG. However, there is an approximately 1.5-hour delay between the closest associated atmospheric pressure extreme and the peak sea level response, possibly suggesting that wave reflection from nearby coastlines may redirect energy into the harbour.

Our research further points that extreme sea level oscillations occur simultaneously relatively often across the network, with the simultaneity index exceeding 50% for most station pairs (Fig. 12). This suggests that large HF sea level oscillations are frequently associated with either same atmospheric disturbances propagating over much of the middle Adriatic, or that intensification of HF atmospheric activity over the middle Adriatic generally occurs simultaneously, likely due to presence of favourable synoptic conditions (Šepić et al., 2015b).

The simultaneity index is lowest for pairs involving Sobra TG. This is likely related to seasonal contrast in its HF oscillations, with smoother and longer-period oscillations (approximately 45–130 minutes; Fig. 2d) more evident during summer and shorter-period oscillations (2–5 minutes) becoming more prominent during winter. If the latter are partly related to infragravity waves (as Sobra is almost an open coast station exposed to open sea waves), their weaker manifestation at other stations could contribute to lower simultaneity. Additionally, lower simultaneity does not imply the absence of a sea level response at another station. An episode may produce substantial oscillations at multiple tide gauges while exceeding the extreme threshold at only few of them, as illustrated in Fig. 8.

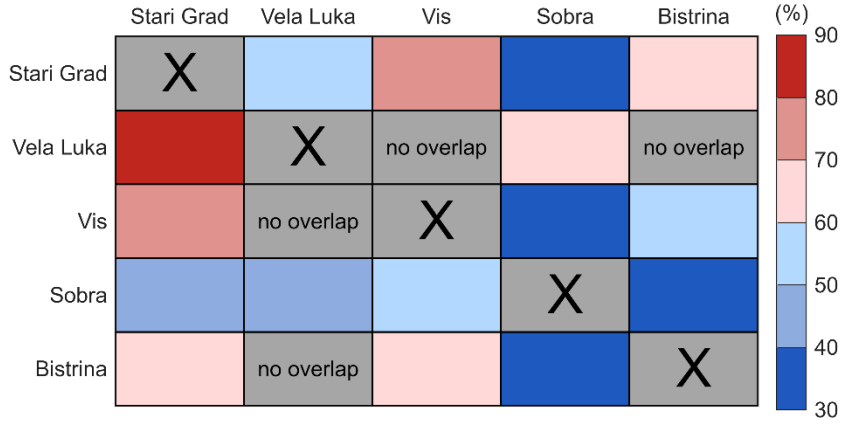


Figure 12. Simultaneity index for sea level extremes, defined as the percentage of extreme episodes at one station that coincide with an extreme episode at another station within a prescribed time window. Stations on the y-axis are the reference stations. Same-station pairs are marked with "X" since the index has no meaning in that case. Cells labelled "no overlap" indicate that the two corresponding tide-gauge stations do not share a common measurement period. The index is directional because it is calculated relative to the number of episodes at the reference station; therefore, differences between opposite directions of a station pair do not imply different physical processes. For example, the lower connection from Stari Grad TG to Vela Luka TG than in the reverse direction mainly reflects differences in the number and magnitude of extreme episodes recorded at the two stations.

In addition to simultaneity of HF sea level extremes, we have also estimated simultaneity of HF air pressure extremes. When considered as a whole, atmospheric pressure extremes show relatively modest simultaneity (Fig. 13, top panel). However, the strongest episodes occur simultaneously over a substantially larger part of the Adriatic (Fig. 13, bottom panel). The $P_{99.99}$ pressure episodes are frequently accompanied by an air pressure extreme at multiple stations, particularly along the eastern Adriatic, where simultaneity generally exceeds 60%. On the western side, values are mostly between 40 and 70%, although

https://doi.org/10.5194/egusphere-2026-6051
Preprint. Discussion started: 18 November 2026
© Author(s) 2026. CC BY 4.0 License.

for Vieste MB they occasionally reach up to 90%. The relationship is also asymmetric: $P_{99.99}$ episodes recorded at Vieste MB are frequently also recorded in Croatia (as either of $P_{99.9}$, $P_{99.95}$ or $P_{99.99}$), whereas the reverse connection is weaker.

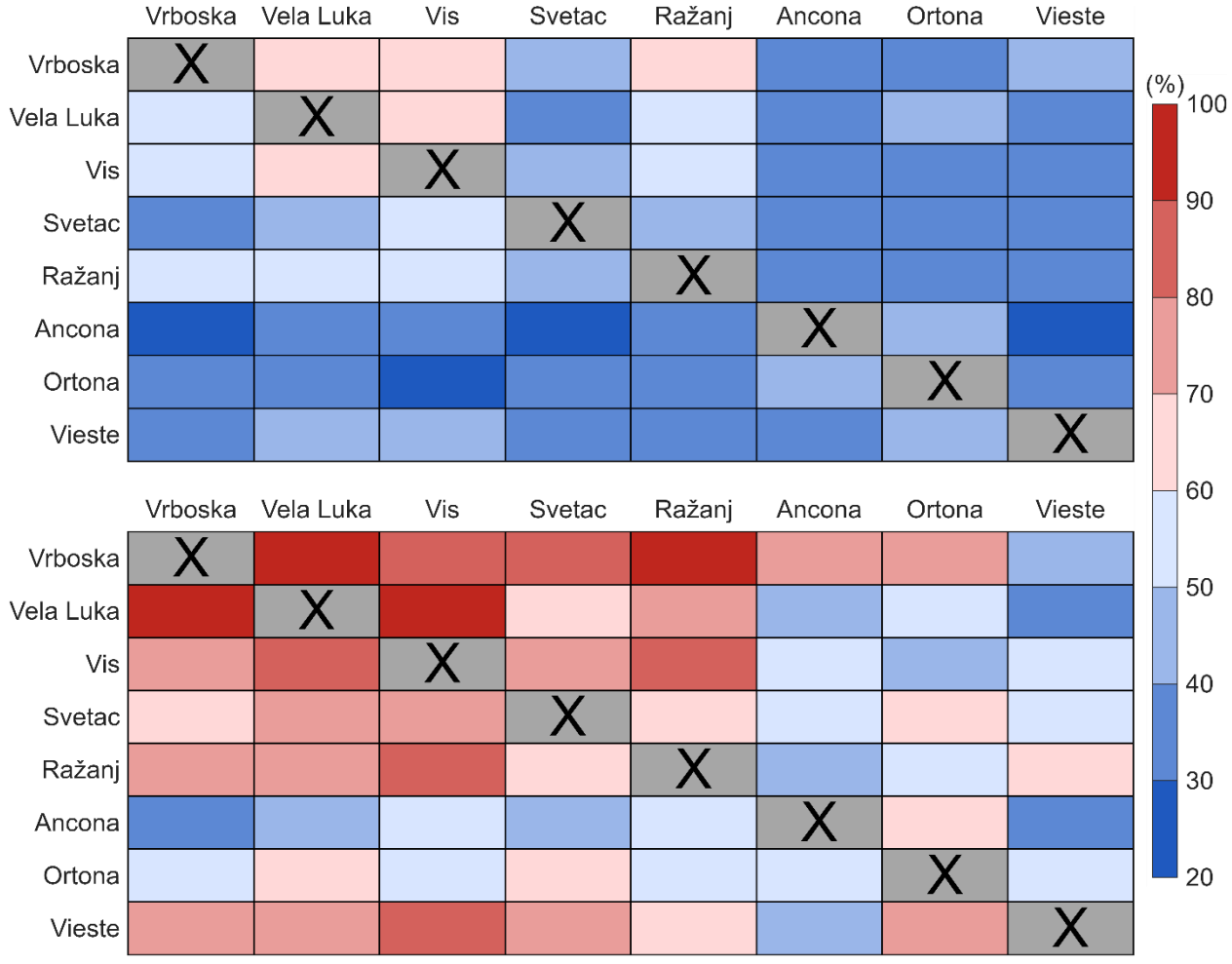


Figure 13. Simultaneity index of (top) all air pressure extremes and (bottom) the strongest ($P_{99.99}$) air pressure extremes. Stations on the y-axis are the reference stations. Same-station pairs are marked with "X".

Finally, we note that in SL→AP direction, only seven unique HF sea level episodes remained unconnected with extreme atmospheric pressure episodes. For these unconnected sea level episodes, between five and eight microbarograph stations were available, yet none recorded an atmospheric pressure extreme. The associated HF atmospheric pressure NMV values were increased for 6 out of 7 episodes (between 3.6 and 7.4 hPa^2), suggesting that more pronounced atmospheric variability was present but remained below the applied extreme threshold. Alternatively, some of these episodes may have been driven or enhanced by wind forcing, which was not considered in the present analysis. It should be noted that out of these seven unique unconnected sea level extremes, five occurred under synoptic conditions considered favourable for generation of HF sea level extremes according to Ruić et al. (2025). These included both the summer-type pattern, characterised by relatively uniform

https://doi.org/10.5194/egusphere-2026-6051
Preprint. Discussion started: 18 November 2026
© Author(s) 2026. CC BY 4.0 License.

mean sea level pressure, southerly warm-air advection at 850 hPa and a jet stream at 500 hPa, and the winter-type pattern, characterised by pronounced mean sea level pressure gradients, a colder lower troposphere and a jet stream at 500 hPa (based on ERA5 Reanalysis – not shown).

Several directions could further extend this study and increase applicability of air pressure measurements for meteotsunami tracking and detection. A denser observational network, with additional microbarographs and tide gauges, would improve the spatial resolution of atmospheric and sea level observations. Longer observational records would provide a larger sample of extreme episodes and strengthen the statistical analysis. Applying isochronal analysis to individual atmospheric disturbances associated with individual sea level episodes would allow their propagation directions and speeds to be estimated more accurately. Numerical hydrodynamic modelling of individual events could also help explain differences in local sea level responses to similar atmospheric disturbances. Data-driven and deep-learning methods could also be explored for forecasting. Together, these approaches could improve understanding of HF sea level extremes and support further development of meteotsunami monitoring and forecasting in the middle Adriatic.

5 Conclusion

The main conclusions of this study are:

1. HF sea level oscillations show substantial spatial variability across the middle Adriatic, with local bathymetry and harbour geometry strongly influencing their magnitude. Bistrina TG exhibits substantially larger extreme wave heights than the other tide gauges, whereas Sobra TG shows the weakest extreme oscillations.
2. Extreme HF sea level episodes are strongly associated with atmospheric pressure disturbances. Between 80 and 100% of the sea level extremes were connected to at least one HF atmospheric pressure extreme, with connection rates generally increasing for stronger sea level episodes, reaching 100% for the highest intensity class at all tide gauges.
3. Atmospheric disturbances associated with extreme sea level episodes predominantly propagate from westerly directions, with estimated median propagation speeds between 12 and 20 m s^{-1}, depending on the tide gauge. These estimates provide a first regional characterisation, although they should be interpreted cautiously given the spatial resolution of the monitoring network and the assumption that the same atmospheric disturbance and the same feature of that disturbance are captured at different microbarograph stations.
4. The reverse connection is considerably weaker, with only 32–45% of extreme atmospheric pressure episodes associated with an extreme sea level response. Thus, strong atmospheric disturbances do not necessarily produce extreme sea level oscillations, indicating that additional conditions are required for a strong sea level response.
5. In both directions, stronger atmospheric pressure disturbances are generally associated with larger HF sea level responses, with median wave heights increasing with atmospheric pressure intensity in most station pairs. However, substantial overlap between intensity classes, together with differences between stations such as Bistrina and Sobra TGs, shows that atmospheric pressure intensity alone is insufficient to explain the observed sea level amplitudes.

https://doi.org/10.5194/egusphere-2026-6051
Preprint. Discussion started: 18 November 2026
© Author(s) 2026. CC BY 4.0 License.

6. The strongest atmospheric disturbances show greater spatial coherence across the Adriatic. Their simultaneity frequently exceeds 60% across the eastern Adriatic, indicating that the most intense disturbances can affect widely separated locations while remaining sufficiently strong to be detected across the network.
7. Five of the seven unconnected sea level extremes occurred under synoptic conditions considered favourable for meteotsunami generation, indicating that the absence of a detected atmospheric pressure extreme does not necessarily imply an absence of atmospheric forcing.

Further studies are needed to better understand the mechanisms controlling individual HF sea level extremes. Episode-specific analyses combining detailed atmospheric observations and hydrodynamic modelling, together with longer and denser tide-gauge and microbarograph records, would help clarify how atmospheric disturbances determine the resulting sea level response. Higher-frequency sea level observations would also help identify the contribution of very short-period oscillations, particularly at Sobra TG. Such developments could ultimately improve the understanding and prediction of extreme HF sea level oscillations and meteotsunami hazards in the Adriatic.

Code and data availability

The 1-minute sea level and air pressure measurements were obtained from IOR (Institute of Oceanography and Fisheries, Split, Croatia). Real time measurements can be seen at http://faust.izor.hr/autodatapub/postaje. The spatial fields from the ERA5 reanalysis are publicly accessible through the Copernicus Climate Change Service Climate Data Store for both single levels (https://doi.org/10.24381/cds.adbb2d47) and pressure levels (https://doi.org/10.24381/cds.bd0915c6).

Author contributions

NM and JŠ contributed to the conceptualisation of the study. NM developed the methodology and performed the analyses, under the supervision of JŠ, who also provided the code for the isochronal analysis method. HM contributed to the initial data analysis. NM wrote the initial draft of the manuscript, JŠ contributed to the interpretation of the results and revised the manuscript and HM provided comments. All authors reviewed and approved the final manuscript.

Competing interests

The authors declare that they have no conflict of interest.

Disclaimer

Copernicus Publications remains neutral with regard to jurisdictional claims made in the text, published maps, institutional affiliations, or any other geographical representation in this paper. While Copernicus Publications makes every effort to include

https://doi.org/10.5194/egusphere-2026-6051
Preprint. Discussion started: 18 November 2026
© Author(s) 2026. CC BY 4.0 License.

appropriate place names, the final responsibility lies with the authors. Views expressed in the text are those of the authors and do not necessarily reflect the views of the publisher.

Acknowledgements

The authors gratefully acknowledge the Institute of Oceanography and Fisheries (IOR), Split, Croatia, for providing the sea level and atmospheric pressure observations used in this study and for maintaining the measurement network.

Financial support

This research has been supported by: ERC projects SHExtreme (853045) and MeD-Track (101213756), Croatian Science Foundation projects "Young Researchers' Career Development Project – Training New Doctoral Students" (DOK-NPOO-2023-10-7076) and CroClimExtremes (IP-2022-10-4144), the STIM–REI 2.0 project (PK.1.1.10.0005), the ZMAJ and KLIMADRIA projects funded by the European Union - NextGenerationEU, the VAL project (PK.3.4.17.0021) funded by the European Regional Development Fund (ERDF).

References

Aucan, J. and Ardhuin, F.: Infragravity waves in the deep ocean: An upward revision, Geophys. Res. Lett., 40, 3435–3439, https://doi.org/10.1002/grl.50321, 2013.

Balić, M. and Šepić, J.: SHELDA: sub-hourly European quality controlled sea level dataset, Earth Syst. Sci. Data, 18, 7143–7179, https://doi.org/10.5194/essd-18-7143-2026, 2026.

Bechle, A. J., Kristovich, D. A. R., and Wu, C. H.: Meteotsunami occurrences and causes in Lake Michigan, J. Geophys. Res. Oceans, 120, 8422–8438, https://doi.org/10.1002/2015JC011317, 2015.

Belušić, D. and Strelec Mahović, N.: Detecting and following atmospheric disturbances with a potential to generate meteotsunamis in the Adriatic, Phys. Chem. Earth Parts ABC, 34, 918–927, https://doi.org/10.1016/j.pce.2009.08.009, 2009.

Belušić, D., Grisogono, B., and Klaić, Z. B.: Atmospheric origin of the devastating coupled air-sea event in the east Adriatic, J. Geophys. Res. Atmos., 112, D17111, https://doi.org/10.1029/2006JD008204, 2007.

Bertin, X., De Bakker, A., Van Dongeren, A., Coco, G., André, G., Ardhuin, F., Bonneton, P., Bouchette, F., Castelle, B., Crawford, W. C., Davidson, M., Deen, M., Dodet, G., Guérin, T., Inch, K., Leckler, F., McCall, R., Muller, H., Olabarrieta, M., Roelvink, D., Ruessink, G., Sous, D., Stutzmann, É., and Tissier, M.: Infragravity waves: From driving mechanisms to impacts, Earth-Sci. Rev., 177, 774–799, https://doi.org/10.1016/j.earscirev.2018.01.002, 2018.

Bubalo, M., Janeković, I., and Orlić, M.: Chrystal and Proudman resonances simulated with three numerical models, Ocean Dyn., 68, 497–507, https://doi.org/10.1007/s10236-018-1146-8, 2018.

https://doi.org/10.5194/egusphere-2026-6051
Preprint. Discussion started: 18 November 2026
© Author(s) 2026. CC BY 4.0 License.

Cushman-Roisin, B. and Naimie, C. E.: A 3D finite-element model of the Adriatic tides, J. Mar. Syst., 37, 279–297, https://doi.org/10.1016/S0924-7963(02)00204-X, 2002.

Denamiel, C., Šepić, J., and Vilibić, I.: Impact of Geomorphological Changes to Harbor Resonance During Meteotsunamis: The Vela Luka Bay Test Case, Pure Appl. Geophys., 175, 3839–3859, https://doi.org/10.1007/s00024-018-1862-5, 2018.

Dodet, G., Melet, A., Ardhuin, F., Bertin, X., Idier, D., and Almar, R.: The Contribution of Wind-Generated Waves to Coastal Sea-Level Changes, Surv. Geophys., 40, 1563–1601, https://doi.org/10.1007/s10712-019-09557-5, 2019.

Greenspan, H. P.: The generation of edge waves by moving pressure distributions, J. Fluid Mech., 1, 574–592, https://doi.org/10.1017/S002211205600038X, 1956.

Haslett, S. K., Mellor, H. E., and Bryant, E. A.: Meteo-tsunami hazard associated with summer thunderstorms in the United Kingdom, Phys. Chem. Earth Parts ABC, 34, 1016–1022, https://doi.org/10.1016/j.pce.2009.10.005, 2009.

Hattori, N., Tajima, Y., Yamanaka, Y., and Kumagai, K.: Study on the influence of infragravity waves on inundation characteristics at Minami-Ashiyahama in Osaka Bay induced by the 2018 Typhoon Jebi, Coast. Eng. J., 62, 182–197, https://doi.org/10.1080/21664250.2020.1724247, 2020.

Heidarzadeh, M. and Rabinovich, A. B.: Combined hazard of typhoon-generated meteorological tsunamis and storm surges along the coast of Japan, Nat. Hazards, 106, 1639–1672, https://doi.org/10.1007/s11069-020-04448-0, 2021.

Hersbach, H., Bell, B., Berrisford, P., Hirahara, S., Horányi, A., Muñoz-Sabater, J., Nicolas, J., Peubey, C., Radu, R., Schepers, D., Simmons, A., Soci, C., Abdalla, S., Abellan, X., Balsamo, G., Bechtold, P., Biavati, G., Bidlot, J., Bonavita, M., De Chiara, G., Dahlgren, P., Dee, D., Diamantakis, M., Dragani, R., Flemming, J., Forbes, R., Fuentes, M., Geer, A., Haimberger, L., Healy, S., Hogan, R. J., Hólm, E., Janisková, M., Keeley, S., Laloyaux, P., Lopez, P., Lupu, C., Radnoti, G., De Rosnay, P., Rozum, I., Vamborg, F., Villaume, S., and Thépaut, J.: The ERA5 global reanalysis, Q. J. R. Meteorol. Soc., 146, 1999–2049, https://doi.org/10.1002/qj.3803, 2020.

Janeković, I. and Kuzmić, M.: Numerical simulation of the Adriatic Sea principal tidal constituents, Ann. Geophys., 23, 3207–3218, https://doi.org/10.5194/angeo-23-3207-2005, 2005.

Jansà, A. and Ramis, C.: The Balearic rissaga: from pioneering research to present-day knowledge, Nat. Hazards, 106, 1269–1297, https://doi.org/10.1007/s11069-020-04221-3, 2021.

Jansà, A., Monserrat, S., and Gomis, D.: The rissaga of 15 June 2006 in Ciutadella (Menorca), a meteorological tsunami, Adv. Geosci., 12, 1–4, https://doi.org/10.5194/adgeo-12-1-2007, 2007.

Lamb, H.: Hydrodynamics, 6th ed., Cambridge University Press, Cambridge, 738 pp., 1932.

Linares, Á., Wu, C. H., Bechle, A. J., Anderson, E. J., and Kristovich, D. A. R.: Unexpected rip currents induced by a meteotsunami, Sci. Rep., 9, 2105, https://doi.org/10.1038/s41598-019-38716-2, 2019.

Medvedev, I. P., Vilibić, I., and Rabinovich, A. B.: Tidal Resonance in the Adriatic Sea: Observational Evidence, J. Geophys. Res. Oceans, 125, e2020JC016168, https://doi.org/10.1029/2020JC016168, 2020.

Medvedev, I. P., Rabinovich, A. B., and Šepić, J.: Destructive coastal sea level oscillations generated by Typhoon Maysak in the Sea of Japan in September 2020, Sci. Rep., 12, 8463, https://doi.org/10.1038/s41598-022-12189-2, 2022.

https://doi.org/10.5194/egusphere-2026-6051
Preprint. Discussion started: 18 November 2026
© Author(s) 2026. CC BY 4.0 License.

Melito, L., Postacchini, M., Sheremet, A., Calantoni, J., Zitti, G., Darvini, G., and Brocchini, M.: Wave-Current Interactions and Infragravity Wave Propagation at a Microtidal Inlet, Proceedings, 2, 628, https://doi.org/10.3390/proceedings2110628, 2018.

Monserrat, S., Vilibić, I., and Rabinovich, A. B.: Meteotsunamis: atmospherically induced destructive ocean waves in the tsunami frequency band, Nat. Hazards Earth Syst. Sci., 6, 1035–1051, https://doi.org/10.5194/nhess-6-1035-2006, 2006.

Munk, W. H.: Surf beats, Eos Trans. Am. Geophys. Union, 30, 849–854, https://doi.org/10.1029/TR030i006p00849, 1949.

Munk, W., Snodgrass, F., and Carrier, G.: Edge Waves on the Continental Shelf, Science, 123, 127–132, https://doi.org/10.1126/science.123.3187.127, 1956.

Nerem, R. S., Beckley, B. D., Fasullo, J. T., Hamlington, B. D., Masters, D., and Mitchum, G. T.: Climate-change–driven accelerated sea-level rise detected in the altimeter era, Proc. Natl. Acad. Sci., 115, 2022–2025, https://doi.org/10.1073/pnas.1717312115, 2018.

Niu, X.: Conditions for the occurrence of notable edge waves due to atmospheric disturbances, Appl. Ocean Res., 101, 102255, https://doi.org/10.1016/j.apor.2020.102255, 2020.

Niu, X.: Resonance of long waves around a circular island and its relation to edge waves, Eur. J. Mech. B Fluids, 86, 15–24, https://doi.org/10.1016/j.euromechflu.2020.11.007, 2021.

Orlić, M.: About a possible occurrence of the Proudman resonance in the Adriatic, Thalass. Jugosl., 16, 79–88, 1980.

Orlić, M.: The first attempt at cataloguing tsunami-like waves of meteorological origin in Croatian coastal waters, Acta Adriat., 56, 83–96, 2015.

Orlić, M., Belušić, D., Janeković, I., and Pasarić, M.: Fresh evidence relating the great Adriatic surge of 21 June 1978 to mesoscale atmospheric forcing, J. Geophys. Res. Oceans, 115, C06011, https://doi.org/10.1029/2009JC005777, 2010.

Pattiaratchi, C. B. and Wijeratne, E. M. S.: Are meteotsunamis an underrated hazard?, Philos. Trans. R. Soc. Math. Phys. Eng. Sci., 373, 20140377, https://doi.org/10.1098/rsta.2014.0377, 2015.

Pawlowicz, R., Beardsley, B., and Lentz, S.: Classical tidal harmonic analysis including error estimates in MATLAB using T_TIDE, Comput. Geosci., 28, 929–937, https://doi.org/10.1016/S0098-3004(02)00013-4, 2002.

Poulain, P.: Tidal currents in the Adriatic as measured by surface drifters, J. Geophys. Res. Oceans, 118, 1434–1444, https://doi.org/10.1002/jgrc.20147, 2013.

Proudman, J.: The Effects on the Sea of Changes in Atmospheric Pressure, Geophys. J. Int., 2, 197–209, https://doi.org/10.1111/j.1365-246X.1929.tb05408.x, 1929.

Pugh, D. and Woodworth, P.: Sea-Level Science: Understanding Tides, Surges, Tsunamis and Mean Sea-Level Changes, 2nd ed., Cambridge University Press, https://doi.org/10.1017/CBO9781139235778, 2014.

Pupić Vurilj, M., Brnas, T., Ruić, K., Šepić, J., and Balić, M.: Mediterranean meteotsunamis of May 2021 and June 2022: Observations, data analysis and synoptic background, Geofizika, 40, 179–205, https://doi.org/10.15233/gfz.2023.40.8, 2023.

Rabinovich, A. B.: Seiches and Harbor Oscillations, in: Handbook of Coastal and Ocean Engineering, edited by: Kim, Y. C., World Scientific, Singapore, 193–236, https://doi.org/10.1142/9789812819307_0009, 2009.

https://doi.org/10.5194/egusphere-2026-6051
Preprint. Discussion started: 18 November 2026
© Author(s) 2026. CC BY 4.0 License.

Rabinovich, A. B.: Twenty-Seven Years of Progress in the Science of Meteorological Tsunamis Following the 1992 Daytona Beach Event, Pure Appl. Geophys., 177, 1193–1230, https://doi.org/10.1007/s00024-019-02349-3, 2020.

Rabinovich, A. B. and Monserrat, S.: Generation of Meteorological Tsunamis (Large Amplitude Seiches) Near the Balearic and Kuril Islands, Nat. Hazards, 18, 27–55, https://doi.org/10.1023/A:1008096627047, 1998.

Raichlen, F.: Harbor resonance, in: Estuary Coastline Hydrodynamics, edited by: Ippen, A. T., McGraw-Hill, New York, 281–340, 1966.

Rasmussen, C. E. and Williams, C. K. I.: Gaussian Processes for Machine Learning, The MIT Press, https://doi.org/10.7551/mitpress/3206.001.0001, 2005.

Ruić, K., Šepić, J., Mlinar, M., and Međugorac, I.: Contribution of high-frequency (T < 2 h) sea level oscillations to the Adriatic sea level maxima, Nat. Hazards, 116, 3747–3777, https://doi.org/10.1007/s11069-023-05834-0, 2023.

Ruić, K., Šepić, J., and Vojković, M.: Synoptic patterns associated with high-frequency sea level extremes in the Adriatic Sea, Ocean Sci., 21, 1183–1203, https://doi.org/10.5194/os-21-1183-2025, 2025.

Seo, S.-N. and Liu, P. L.-F.: Edge waves generated by atmospheric pressure disturbances moving along a shoreline on a sloping beach, Coast. Eng., 85, 43–59, https://doi.org/10.1016/j.coastaleng.2013.12.002, 2014.

Šepić, J. and Orlić, M.: Adriatic Meteotsunami Catalogue, https://projekti.pmfst.unist.hr/floods/meteotsunamis/, last access: 19 August 2026.

Šepić, J. and Rabinovich, A. B.: Meteotsunami in the Great Lakes and on the Atlantic coast of the United States generated by the “derecho” of June 29–30, 2012, Nat. Hazards, 74, 75–107, https://doi.org/10.1007/s11069-014-1310-5, 2014.

Šepić, J. and Vilibić, I.: The development and implementation of a real-time meteotsunami warning network for the Adriatic Sea, Nat. Hazards Earth Syst. Sci., 11, 83–91, https://doi.org/10.5194/nhess-11-83-2011, 2011.

Šepić, J., Vilibić, I., and Belušić, D.: Source of the 2007 Ist meteotsunami (Adriatic Sea), J. Geophys. Res. Oceans, 114, C03016, https://doi.org/10.1029/2008JC005092, 2009.

Šepić, J., Vilibić, I., and Strelec Mahović, N.: Northern Adriatic meteorological tsunamis: Observations, link to the atmosphere, and predictability, J. Geophys. Res. Oceans, 117, C02002, https://doi.org/10.1029/2011JC007608, 2012.

Šepić, J., Vilibić, I., and Fine, I.: Northern Adriatic meteorological tsunamis: Assessment of their potential through ocean modeling experiments, J. Geophys. Res. Oceans, 120, 2993–3010, https://doi.org/10.1002/2015JC010795, 2015a.

Šepić, J., Vilibić, I., Rabinovich, A. B., and Monserrat, S.: Widespread tsunami-like waves of 23-27 June in the Mediterranean and Black Seas generated by high-altitude atmospheric forcing, Sci. Rep., 5, 11682, https://doi.org/10.1038/srep11682, 2015b.

Šepić, J., Međugorac, I., Janeković, I., Dunić, N., and Vilibić, I.: Multi-Meteotsunami Event in the Adriatic Sea Generated by Atmospheric Disturbances of 25–26 June 2014, Pure Appl. Geophys., 173, 4117–4138, https://doi.org/10.1007/s00024-016-1249-4, 2016.

Thomson, R. E. and Emery, W. J.: Data Analysis Methods in Physical Oceanography, 4th ed., Elsevier, ISBN 978-0-323-91723-0, 2024.

https://doi.org/10.5194/egusphere-2026-6051
Preprint. Discussion started: 18 November 2026
© Author(s) 2026. CC BY 4.0 License.

Thomson, R. E., Rabinovich, A. B., Fine, I. V., Sinnott, D. C., McCarthy, A., Sutherland, N. A. S., and Neil, L. K.: Meteorological tsunamis on the coasts of British Columbia and Washington, Phys. Chem. Earth Parts ABC, 34, 971–988, https://doi.org/10.1016/j.pce.2009.10.003, 2009.

Tojčić, I., Denamiel, C., and Vilibić, I.: Performance of the Adriatic early warning system during the multi-meteotsunami event of 11–19 May 2020: an assessment using energy banners, Nat. Hazards Earth Syst. Sci., 21, 2427–2446, https://doi.org/10.5194/nhess-21-2427-2021, 2021.

Vilibić, I.: Numerical simulations of the Proudman resonance, Cont. Shelf Res., 28, 574–581, https://doi.org/10.1016/j.csr.2007.11.005, 2008.

Vilibić, I. and Beg Paklar, G.: High-frequency atmospherically-induced oscillations in the middle Adriatic coastal area, Ann. Geophys., 24, 2759–2771, https://doi.org/10.5194/angeo-24-2759-2006, 2006.

Vilibić, I. and Šepić, J.: Destructive meteotsunamis along the eastern Adriatic coast: Overview, Phys. Chem. Earth Parts ABC, 34, 904–917, https://doi.org/10.1016/j.pce.2009.08.004, 2009.

Vilibić, I. and Šepić, J.: Global mapping of nonseismic sea level oscillations at tsunami timescales, Sci. Rep., 7, 40818, https://doi.org/10.1038/srep40818, 2017.

Vilibić, I., Domijan, N., Orlić, M., Leder, N., and Pasarić, M.: Resonant coupling of a traveling air pressure disturbance with the east Adriatic coastal waters, J. Geophys. Res. Oceans, 109, 2004JC002279, https://doi.org/10.1029/2004JC002279, 2004.

Vilibić, I., Šepić, J., Rabinovich, A. B., and Monserrat, S.: Modern Approaches in Meteotsunami Research and Early Warning, Front. Mar. Sci., 3, 57, https://doi.org/10.3389/fmars.2016.00057, 2016.

Vilibić, I., Denamiel, C., Zemunik, P., and Monserrat, S.: The Mediterranean and Black Sea meteotsunamis: an overview, Nat. Hazards, 106, 1223–1267, https://doi.org/10.1007/s11069-020-04306-z, 2021.

Vilibić, I., Zemunik Selak, P., and Šepić, J.: Meteorological Tsunamis: From Local Hazard to Global Relevance, Rev. Geophys., 63, e2024RG000867, https://doi.org/10.1029/2024RG000867, 2025.

Villalonga, J., Monserrat, S., Gomis, D., and Jordà, G.: Observational Characterization of Atmospheric Disturbances Generating Meteotsunamis in the Balearic Islands, J. Geophys. Res. Oceans, 129, e2024JC020910, https://doi.org/10.1029/2024JC020910, 2024.

Villalonga, J., Pascual, J., Puigdefàbregas, J., Gomis, D., and Jordà, G.: Meteotsunamis in the Western Mediterranean: a regional analysis from high-frequency sea level observations, Nat. Hazards, 122, 133, https://doi.org/10.1007/s11069-025-07801-3, 2026.

Vučetić, T., Vilibić, I., Tinti, S., and Maramai, A.: The Great Adriatic flood of 21 June 1978 revisited: An overview of the reports, Phys. Chem. Earth Parts ABC, 34, 894–903, https://doi.org/10.1016/j.pce.2009.08.005, 2009.

Wijeratne, E. M. S. and Pattiaratchi, C. B.: Meteotsunamis Generated by Thunderstorms, J. Geophys. Res. Oceans, 129, e2023JC020662, https://doi.org/10.1029/2023JC020662, 2024.

Williams, J., Matthews, A., and Jevrejeva, S.: Development of an automatic tide gauge processing system, National Oceanography Centre Research and Consultancy Report, 64, National Oceanography Centre, Southampton, 26 pp., 2019.

https://doi.org/10.5194/egusphere-2026-6051
Preprint. Discussion started: 18 November 2026
© Author(s) 2026. CC BY 4.0 License.

Woodworth, P. L., Menéndez, M., and Roland Gehrels, W.: Evidence for Century-Timescale Acceleration in Mean Sea Levels and for Recent Changes in Extreme Sea Levels, Surv. Geophys., 32, 603–618, https://doi.org/10.1007/s10712-011-9112-8, 2011.

Zemunik, P., Šepić, J., Pellikka, H., Ćatipović, L., and Vilibić, I.: Minute Sea-Level Analysis (MISELA): a high-frequency sea-level analysis global dataset, Earth Syst. Sci. Data, 13, 4121–4132, https://doi.org/10.5194/essd-13-4121-2021, 2021.